의학박사 학위논문

Time-averaged simulated microgravity (taSMG) using a 3D clinostat induces autophagy via mitochondrial dysfunction in human Hodgkin's lymphoma cells

3 차원 클리노스탯을 이용한 시간-평균 미세중력 모사 환경이 유도하는 인간 호지킨 림프종세포의 미토콘드리아 기능 장애와 자가 포식

2020 년 8 월

서울대학교 대학원
의과학과 의과학전공
정 애 진

A thesis of the Degree of Doctor of Philosophy

3 차원 클리노스탯을 이용한 시간-평균 미세중력 모사 환경이 유도하는 인간 호지킨 림프종세포의 미토콘드리아 기능 장애와 자가 포식

Time-averaged simulated microgravity (taSMG) using a 3D clinostat induces autophagy via mitochondrial dysfunction in human Hodgkin's lymphoma cells

August 2020

The Department of Biomedical Sciences
(Major in Biomedical Sciences)
Seoul National University
College of Medicine
Ae Jin Jeong

학위논문 원문제공 서비스에 대한 동의서

본인의 학위논문에 대하여 서울대학교가 아래와 같이 학위논문 제공하는 것에 동의합니다.

1. 동의사항

① 본인의 논문을 보존이나 인터넷 등을 통한 온라인 서비스 목적으로 복제할 경우 저작물의 내용을 변경하지 않는 범위 내에서의 복제를 허용합니다.

② 본인의 논문을 디지털화하여 인터넷 등 정보통신망을 통한 논문의 일부 또는 전부의 복제.배포 및 전송 시 무료로 제공하는 것에 동의합니다.

2. 개인(저작자)의 의무

본 논문의 저작권을 타인에게 양도하거나 또는 출판을 허락하는 등 동의 내용을 변경하고자 할 때는 소속대학(원)에 공개의 유보 또는 해지를 즉시 통보하겠습니다.

3. 서울대학교의 의무

① 서울대학교는 본 논문을 외부에 제공할 경우 저작권 보호장치(DRM)를 사용하여야 합니다.

② 서울대학교는 본 논문에 대한 공개의 유보나 해지 신청 시 즉시 처리해야 합니다.

논문 제목: Time-averaged simulated microgravity (taSMG) using a 3D clinostat induces autophagy via mitochondrial dysfunction in human Hodgkin's lymphoma cells

학위구분: **석사** □ **박사** ■
학 과: 의과학과
학 번: 2015-30609
연 락 처: 010-9798-5998
저 작 자: 정 애 진 (서명)

제 출 일: 2020 년 7 월 30 일

서울대학교총장 귀하

ABSTRACT

Gravitational forces can impose physical stresses on the human body as it functions to maintain homeostasis. It has been reported that astronauts exposed to microgravity experience altered biological functions and many subsequent studies on the effects of microgravity have therefore been conducted. Many studies are being conducted using Clinostat, a system that provides an environment that simulates microgravity on Earth. However, the mechanisms of various cytological changes in simulated microgravity is still unclear. So, this study observed changes in human Hodgkin's lymphoma (HL) cells using 3D clinostat, which provides a time-averaged simulated microgravity (taSMG). It was observed that the cell growth of HL cells was inhibited when cultured in taSMG for 3 days, whereas it did not affect normal human dermal fibroblast (HDF) cells. And then, to confirm that taSMG has anticancer effects, HL cells were exposed to taSMG for 2 days. While reactive oxygen species (ROS) production and NADPH oxidase family gene expression were increased, mitochondrial mass, ATPase, ATP synthase, and intracellular ATP levels were decreased.

Furthermore, human HL cells exposed to taSMG underwent autophagy via AMPK/Akt/mTOR and MAPK pathway modulation; such autophagy was inhibited by the ROS scavenger *N*-acetylcysteine (NAC). As space travel or more advanced methods of simulating microgravity on Earth have been developed, these findings suggest that it is valuable as a new treatment for HL instead of conventional chemotherapy and radiotherapy.

Keywords: Gravity, 3D clinostat, Time-averaged simulated microgravity, Hodgkin's lymphoma, Mitochondrial dysfunction, ROS generation, Autophagy

Student number: 2015-30609

CONTENTS

LIST OF FIGURES

LIST OF ABBREVIATIONS

International space station (ISS)

taSMG: time-averaged simulated microgravity

HL: Hodgkin's lymphoma

HDF: human dermal fibroblast

ROS: reactive oxygen species

NADPH: nicotinamide adenine dinucleotide phosphate

NAC: *N*-acetylcysteine

PI3K: phosphoinositide 3-kinase

mTOR: mammalian target of rapamycin

AMPK: adenosine monophosphate-activated protein kinase

ULK1: Unc-51 like autophagy activating kinase 1

PTEN: phosphatase and tensin homolog

ERK: extracellular signal-regulated kinase

JNK: c-Jun N-terminal kinase

MAPK: mitogen-activated protein kinase

PARP: poly (ADP-ribose) polymerase

ATG14: autophagy related 14

ATF4: activating transcription factor 4

LC3: microtubule-associated protein 1 light chain 3

LKB1: liver kinase B1

Bcl-2: B-cell lymphoma 2

Mcl-1: myeloid cell leukemia 1

Δx Δy Δz: position deviation from clinostat center with respect to Local 2 frame

RT-PCR: reverse transcription-polymerase chain reaction

qRT-PCR: quantitative real-time-polymerase chain reaction

ATP: adenosine triphosphate

FACS: fluorescence activated cell sorter

SEM: standard error of the mean

INTRODUCTION

The advent of human space exploration has produced novel research in to the effects of space travel on human health and diseases. In space, microgravity and cosmic radiation are considered the most consequential environmental factors [1, 2]. Several studies have found that astronauts and experimental animals in space experience physiological changes owing to microgravity during and after space flights; the effects of microgravity include muscle atrophy, bone loss, immune dysregulation, and abnormal cellular functions [3–8]. These findings strongly indicate that the human body experiences physiological changes under microgravity. The international space station (ISS) has a microgravity laboratory and is actively conducting a wide variety of studies, including changes in the human body due to microgravity (Figure 1) [9–13].

However, this is extremely challenging to study in vivo as microgravity is difficult to simulate; as such, long-term exposure to microgravity (10^{-4} G, 1 G is defined as 9.8 m/s^2) may be experienced in space. Therefore, an alternative strategy, termed time-averaged simulated microgravity (taSMG), has been proposed, wherein a continuous change in the direction of gravity enables simulation of the effect of microgravity on cells.

Previous studies have demonstrated that certain types of cells, such as leukocytes (human leukemic myelomonocytic cell line U937) [14, 15] and T lymphocytes [16–18], show similar results when exposed to real microgravity and taSMG.

Accordingly, clinostats have been utilized to provide taSMG as an alternative of real microgravity condition despite physically different situation in which they are under.

Microgravity also affects major cellular functions such as cell growth, cell cycle, self-renewal and differentiation [7, 19-22]. As such, it was hypothesized that microgravity has anticancer potential and many studies were conducted to investigate this notion. So far as it is known, simulated microgravity inhibits proliferation and migration in malignant glioma cell and nonsmall cell lung cancer cell [2, 23]. And simulated microgravity regulates PTEN/FOXO3/AKT pathway, causing cell death and morphogenetic differentiation in colorectal cancer cells [24]. In addition, simulated microgravity promotes cell apoptosis by regulating the DNA-damage response pathway in BL6-10 melanoma cells [25]. Furthermore, simulated microgravity regulates spheroid formation [26, 27], loses stemness of lung cancer stem cells [21], and promotes chemosensitivity of malignant glioma cell [2].

Microgravity also has been reported to cause cellular oxidative stress that leads to the production of reactive oxygen species (ROS), as well as endoplasmic reticulum stress [22, 28-30]. However, the mechanism by which microgravity elicits these cellular responses remain poorly understood.

Autophagy is a catabolic process that helps maintain cellular homeostasis through the degradation of bulk cytoplasm, long-lived proteins, and organelles in response to stresses such as nutrient deprivation, viral infection, and genotoxicity [31-33]. Recent evidence suggests that autophagy is an important

mediator of pathological response and of the cell's response to oxidative stress caused by ROS and reactive nitrogen species [34–36]. Autophagy involves the formation of double–membrane–bound structures called autophagosomes as initiated by the phosphoinositide 3–kinase (PI3K) type III–Atg6/Beclin–1 cascade [37, 38]. The classic PI3K/Akt/mammalian target of rapamycin (mTOR) signaling pathway is an important negative regulator of autophagosome formation. Recent studies have found that activation of adenosine monophosphate–activated protein kinase (AMPK) results in autophagy via the negative regulation of mTOR and direct phosphorylation of Unc–51 like autophagy activating kinase 1 (ULK1) [39–41]. The role of autophagy induction in cells is depend on the nature of the stimulus as well as the cell type.

In cancer therapy, autophagy increases cell migration, invasion, and chemoresistance, paradoxically autophagy can also induce cell death in response to certain stimuli and causes dysregulated cell energy metabolism [42–47]. Therefore, it is necessary to fully understand the function and mechanism of autophagy in cancer therapy.

Hodgkin's lymphoma (HL) is a malignant tumor originating from B cells, while its precise cause is unknown, approximately 9,000 new patients are diagnosed annually in the United States [48]. HL is more common in males than in females, and most commonly occurs in individuals aged 15–40 or over 50 years but rarely in those under 10 years. If diagnosed found at an early stage, it can be treated with chemotherapy or radiotherapy, whereupon the 5–year survival rate is as high as 86%. Classical

therapies have greatly improved the chance of cure, although their side effects are often severe [49–51]. Furthermore, recurrence after successful treatment is common [52–57]. Therefore, novel anticancer therapies that avoid the severe side effects and recurrence rates of existing modalities are needed.

In the present study, I simulated a time–averaged microgravity environment to investigate if such a milieu produces an anticancer effect against human HL cells. The time–averaged simulated microgravity (taSMG) environment was produced using a clinostat as validated [58]. The clinostat rotates in a manner that produces a constantly varying gravity vector in a non–repeating pattern, thereby producing a vector–free gravity environment by continuously averaging the vector. Using a clinostat can provide gravitational stress and microgravity–like effects in cells.

First of all, it has been observed that exposure to taSMG elicits physiological changes in the growth of human HL cells, but not that of normal HDF cells [58]. In addition, taSMG showed growth inhibition in human breast cancer cells.

And then, it has been hypothesized that taSMG produces cellular stress in human HL cells. Among various cellular stress factors, ROS production was investigated because it was known that the microgravity induces oxidative stress [28, 30]. It was confirmed that taSMG increased ROS generation and mitochondrial dysfunction in human HL cells, but there was no change in normal HDF cells. Also, these results are defended in NAC treatment, which is a ROS scavenger. As a results, it was found that taSMG induces autophagy through mitochondrial

dysregulation via the AMPK/Akt/mTOR and MAPK pathways in human HL cells [59].

MATERIALS AND METHODS

This section provides information on the cells and materials used in this study and lists the 3D clinostat production process and simulation and experimental methods.

1. Cell culture

Human Hodgkin's lymphoma (HL) cell lines L-540 and HDLM-2 were obtained from the German Collection of Microorganisms and Cell Cultures (DSMZ, Braunschweig, Germany) [60]. Human dermal fibroblast (HDF) cells, human breast cancer cell lines MCF7 and MDA-MB-231, murine pro-B cell line Ba/F3 and human natural killer cell line NK-92 were purchased from the American Type Culture Collection (ATCC, Manassas, VA, US).

L-540, HDLM-2, HDF and Ba/F3 cells were maintained in RPMI 1640 (Life Technologies, USA) supplemented with 10% fetal bovine serum (FBS, Life Technologies) and 1% penicillin/streptomycin solution (P/S, Life Technologies) at 37℃ in 5% CO_2. MCF7 and MDA-MB-231 cells were maintained in DMEM (Life Technologies) supplemented with 10% FBS and 1% P/S solution at 37℃ in 5% CO_2.

NK-92 cells were maintained in alpha minimum essential medium with 100 U/ml recombinant IL-2 (Sigma Aldrich, USA), 20% FBS and 1% P/S solution at 37℃ in 5% CO_2.

For cellular ROS inhibition, the cells were added with *N*-acetylcysteine (NAC, Sigma Aldrich) at 10 mM in complete

medium for operating clinostat.

2. 3D clinostat development

The 3D clinostat hardware was designed and manufactured according to a conventional 3D clinostat structure (Figure 2) [58]. The clinostat used in this study consists of two perpendicular frames that can rotate independently. The structure of the 3D clinostat was designed using the CAD program (SolidWorks, Dassault Systemes, France, using Seoul National University Academic License) and manufactured using a milling machine with aluminum plates. Two motors (MX-64T, ROBOTIS, Seoul, Republic of Korea) were used to actuate the two frames of the clinostat. Electrical wires for power supply and communication were connected via slip ring, which enables electrical connection between external and rotating frames.

The dimensions of the clinostat were limited to 300 × 310 × 350 mm (length × width × height) as the hardware was to be operated within an incubator for cell proliferation. A mechanical stage, which fixes 25 cm^2 flasks (SPL Life Sciences Co, Korea) for cell cultivation and is capable of accommodating a maximum of eight flasks simultaneously, was affixed at the center of the clinostat (Figure 2) [58]. The quantitative dimensions of the mechanical stage relative to its center of rotation are provided in Figure 3 [58].

The clinostat was controlled by a control algorithm embedded in an external personal computer. The control algorithm provided constant angular velocities for two actuators; the angular velocities were determined by considering the

symmetric distribution of the acceleration vector, which consists of the gravitational acceleration and non-gravitational acceleration. The optimal angular velocities were determined according to simulation based on the kinematic model.

A graphical user interface was implemented using LabVIEW 2009 (National Instruments, Austin, TX, USA, using Seoul National University Academic License) for convenient and stable operation (Figure 4) [58].

3. Operating 3D clinostat

Cells were seeded in 25 cm^2 flasks at a density of 100,000 cells/ml and incubated overnight. Before being placed on the clinostat, the flasks were carefully filled with medium without air bubbles in order to avoid shearing of the cell surface.

After the flasks were fixed on the stage of the clinostat, the clinostat was operated for 1, 2, and 3 days in a commercially available incubator set at 37℃ and supplied with 5% CO_2. The cells grown in parallel at 1 G comprised the control culture, which was kept statically in the same incubator as the clinostat.

4. Cell number analysis

Cell counting was performed manually with a hemocytometer (Biosystems, Nunningen, Switzerland) on trypan blue (Life Technologies) treated cells to assess cell concentration and viability, according to the dye exclusion method. The counts were carried out in triplicate per independent sample.

5. ROS detection assay

For detection of cellular ROS, I used DCFDA cellular ROS detection assay kit (Abcam, UK). The collected cells were stained with 20 μM DCFDA in 1X buffer for 30 min at 37℃. Without the washing procedure, stained cells were immediately carried out by flow cytometry (FACS) using FACS LSRFortessa (BD Bioscience, USA) at Ex488 nm/Em535 nm beam. Each determination was based on the mean fluorescence intensity of 10,000 cells.

6. Mitochondrial mass analysis

Mitochondrial mass per cell was measured by flow cytometry using MitoTracker Green FM (Thermo Fisher Scientific, USA). Cells were collected, resuspended in 0.5 ml of PBS, and stained with 40 nM MitoTracker green (MTG) for 15 min at 37℃ in the dark. Cells were then washed with PBS, resuspended in FACS buffer (eBioscience, USA), and added 200 ng/ml of DAPI (Sigma Aldrich). Stained cells were analyzed using FACS LSRFortessa at Ex488 nm/Em535 nm beam. Each determination was based on the mean fluorescence intensity of 25,000 cells

7. Reverse transcription (RT)-PCR and quantitative real-time RT-PCR (qRT-PCR)

Total RNA were extracted using a RNAiso Plus reagent (Takara, Japan) and cDNA was synthesized using ReverTra Ace qPCR RT Master Mix kit (TOYOBO, Japan). Quantitative real time-PCR was performed using the SYBR Green PCR mix (Applied Biological Material, Canada) with an Applied

Biosystems 7300 Real-time PCR system (Life Technologies) and the raw data were analyzed using comparative Ct quantification. All primers were purchased from Qiagen (Qiagen, USA). The as basic PCR amplification conditions were 58°C annealing temperature and 35 cycles.

8. ATP assay

Levels of intracellular ATP was measured using an ATP Bioluminescence assay kit (Roche, Switzerland) according to manufacturer's instruction. Cells were collected and heated tubes to at least 95°C for 7 min. To remove pellet cell debris, spin down at 14000 RPM for 3 min. And then each sample were transferred to a black 96 well plate and quickly added luciferase reagent to each well. Luminescence was measured at 0.1 sec/well using the luminescence program.

9. Western blot

Cells were lysed in a lysis buffer (50 mM Tris-HCl, pH 7.4, 350 mM NaCl, 0.5% NonidetP-40, 10% glycerol, 0.1% SDS, and 1% Triton X-100). The lysates were centrifuged at 13200 rpm for 10 min at 4°C and protein amounts were quantified using a Bio-Rad protein assay (Bio-Rad, USA). Proteins were separated by SDS-poly acrylamide gel electrophoresis (SDS-PAGE) and transferred onto nitrocellulose membranes (Whatman, Atlanta, USA). The membranes were blocked in blocking buffer (5% skim milk in 150 mM NaCl, 25 mM Tris-HCl, pH 7.4, and 0.1% Tween 20) and subsequently incubated with specific primary antibodies for the target molecules. The

membranes were then washed with Tris-buffered saline containing 0.1% Tween 20 (TBS-T) and further incubated with horseradish peroxidase (HRP)-conjugated secondary antibodies for 1 h at room temperature. After washing with TBS-T, the signals were visualized using the ECL Plus Western blotting substrate (Thermo Fisher Scientific).

10. Statistical analysis.

All experiments were performed by more than four times. The results are represented as means with standard error of the mean (SEM). Statistical significance was determined based on a two-tailed Student's t-test and analyzed using Graph Pad Prism 6 (Graph Pad Software, INC., USA).

In this section, the cells and experimental materials used in this study were provided, and the 3D clinostat development and operation process were described. In addition, experimental techniques and methods such as cell number analysis, ROS detection assay, mitochondrial mass analysis, RT-PCR, qRT-PCR, ATP assay, and western blot were described. All experiments were performed at least 3 times per independent sample.

RESULTS

In this section, a 3D clinostat simulation and time-averaged simulated microgravity are described to determine the effect of the various cells. Since the use of 3D clinostat in this study is a new attempt, various experiments have been conducted to establish appropriate experimental conditions.

1. 3D Clinostat simulation

The optimization approach, using the Taguchi method, enabled angular velocities of the outer and inner frame to reach 0.913 and 0.683 rpm, respectively. The angular velocities are less than 5.5°/s and the mechanical condition inside rotating flasks can be approximated to quasi-static state. Thus, it can be assumed that mechanical condition inside rotating flasks is similar to that of stationary flasks. The combination of the two angular velocities showed symmetric acceleration distribution, as shown in Figure 5 [58].

Using the two optimized angular velocities, simulation of microgravity using the 3D clinostat was performed, and acceleration for 24 h was calculated for validation. A point with relative position [Δx Δy Δz] = [0.1 m 0.1 m 0.1 m] measured from the center of the clinostat was assumed. Assumed relative position is further away center of rotation more than any other points of the flasks fixed in stage. Since residual acceleration, which interrupts nullification of gravity, increases as distance

from center of rotation becomes farther, the position [0.1 m 0.1 m 0.1 m] is appropriate for reliable simulation.

The gravitational, centrifugal, and tangential accelerations were considered in calculation of time-averaged acceleration, which indicates taSMG, as shown in Figure 6 [58]. As shown in figure, time-averaged acceleration decreases as damped oscillation for 1 h. After 24 h, the time-averaged acceleration, which consists of the gravitational and non-gravitational acceleration vectors, enabled the 3D clinostat to provide the condition of 1.7×10^{-4} G.

The time-averaged gravitational acceleration also decreased with damped oscillation, as shown in Figure 7A, and reached 3.3×10^{-4} G after 24 h. The time-averaged gravitational acceleration decreased and asymptoted to zero with time; however, the time-averaged non-gravitational acceleration did not demonstrate a decreasing tendency and was relatively constant (Figure 7B). After 24 h, time-averaged non-gravitational acceleration reached 1.7×10^{-4} G, which is almost the same value as that of the initial state [58].

2. Cell culture conditions in 3D clinostat culture system

In order to reduce the shearing flow stress in the 3D clinostat culture system, the cells are incubated with media full-filled in a 25 cm^2 flask. Therefore, it was necessary to compare the cellular response between the half-filled and full-filled media conditions. First, cell growth was confirmed under half- and full-filled media conditions, and cell growth was slightly inhibited in full-filled compared to half-filled media condition (Figure 8A).

However, in the half-filled media condition, it is considered that the effect of taSMG cannot be confirmed because the shearing flow stress during 3D clinostat operation. Therefore, it was conducted under the premise that it may be different from these normal cell culture conditions.

To the next, to check whether the gas exchange was well performed, the media pH was measured, and it was confirmed that the gas exchange was sufficiently performed even in the full-filled media condition (Figure 8B).

3. taSMG inhibits the cell growth in human HL cell lines

taSMG is known to affect various cellular processes [61-63]. In order to investigate whether taSMG elicits varying physiological changes in tumor cells relative to normal cells, I examined the cell viability of human HL cells (L-540 and HDLM-2 cells) and normal HDF cells regulated under taSMG. After cell culture under taSMG for 1, 2, and 3 days, cell proliferation was analyzed. The taSMG was found to inhibit the cell viability of L-540 and HDLM-2 cells, but did not affect the growth of HDF cells (Figure 9A-C)[58]. These data indicate that taSMG selectively inhibits cell growth in human lymphoma cells, but not in normal cells. Additionally, when L-540 and HDLM-2 cells under taSMG were compared, growth of L-540 cells was inhibited to a larger extent than that of HDLM-2 cells (Figure 9D) [59].

Since HL cells are suspended cells and HDF cells are adherent cells, I wondered whether these conditions are affected by taSMG differently. Under the same experimental conditions,

it was confirmed that human breast cancer cell line MCF7 and MDA-MB-231 cells, which are adherent cancer cells, were inhibited by taSMG (Figure 10).

In addition, human NK cell line (NK-92) and murine pro-B cell line (Ba/F3), which are suspension cells and not cancer cells, were confirmed with the same experimental conditions. Because clinostat culture system cannot replace the media, IL-2-dependent NK-92 cells were processed for up to 2 days only. Unexpectedly, cell growth was inhibited in NK-92 cells and increased in Ba/F3 cells in taSMG condition (Figure 11).

4. taSMG induces mitochondrial dysfunction in human HL cells

In taSMG conditions, the growth of human HL cells is inhibited, and since it has been reported that cell proliferation is mediated by mitochondrial regulation [64-66], I investigated whether taSMG induces mitochondrial stress in human HL cells.

I found that intracellular ROS levels were increased under taSMG compared to normal gravity, 1 G (Figure 12A) [59]. As ROS is generated by nicotinamide adenine dinucleotide phosphate (NADPH) oxidase [67-69], I also found that the expression levels of NADPH oxidase family genes (*gp91-*, *p22-*, *p47-*, and *p67-phox*) are higher under taSMG than under 1 G conditions (Figure 12B) [59]. To observe changes in mitochondrial biogenesis, I measured the mitochondrial mass using MitoTracker labeling and found it to be significantly decreased under taSMG (Figure 13A) [59].

Furthermore, the mRNA expression levels of ATPase (*ATP1A1*) and ATP synthase (*ATP5A1*) were notably lower

than 1 G levels, as determined by RT-PCR and qRT-PCR (Figure 13B and C) [59]. These findings confirmed that intracellular ATP levels were significantly lower under taSMG than 1 G (Figure 13D) [59]. These results suggest that taSMG causes ROS generation and mitochondrial dysfunction in human HL cells.

Unlike human HL cells, ROS generation and reduction of mitochondrial mass by taSMG were not induced in HDF cells (Figure 14A and B). Therefore, taSMG suggests that cancer cells may be more sensitive than normal cells.

5. Mitochondrial dysregulation under taSMG leads to human HL cell autophagy

Mitochondrial dysfunction, as evidenced by increased ROS generation and reduced ATP levels, triggers autophagy [32, 34, 70]. Therefore, I measured the expression levels of the autophagy-related genes (*ULK1, ATG14, BECN1* and *MAP1LC3A*); all were found to be upregulated under taSMG (Figure 15A and B) [59]. Levels of phosphorylated ULK1, ATF4, Beclin-1, and microtubule-associated protein 1 light chain 3 (LC3) were increased, while expression of the Bcl-2 family proteins Bcl-2 and Mcl-1, which inhibit autophagy by directly binding to the BH3 domain of Beclin-1/Atg6, were decreased under taSMG conditions (Figure 15C) [59]. Additionally, I found that the LC3-II/I ratio [71-73], an indicator of autophagy, increased under taSMG (Figure 15D) [59]. These results showed that taSMG contributes to the induction of autophagy in human HL cells.

6. AMPK/Akt/mTOR and MAPK signaling are differentially regulated under taSMG

To further understand the mechanism of taSMG-induced autophagy, various cell signaling pathways by Western blotting were investigated. Since the liver kinase B1 (LKB1)/AMPK pathway is known to be activated under conditions of low intracellular ATP to inhibit cell growth and induce autophagy [74], It was confirmed that activation of these pathway occurs in taSMG. It was found that LKB1 and activated AMPK were increased under taSMG (Figure 16A) [59]. It has been confirmed that activated AMPK inhibits the Akt/mTOR/S6K pathway (a negative regulator of autophagy) and activates the Akt suppressor protein PTEN (Figure 16A) [59]. Previous studies have shown that ROS activates MAPK signaling, and that this elicits a variety of downstream signaling events [75-77]. To that end, I found that taSMG activates RAS, ERK, and JNK (Figure 16B) [59].

Additionally, ROS-induced JNK and ERK activation are known to induce both autophagy and apoptosis [78]. So, it was investigated that cleaved PARP, caspase-3 and -9 as apoptosis markers, and it was proved that taSMG does not induce apoptosis (Figure 17) [59]. These results suggest that only autophagy is induced by modulating the AMPK/Akt/mTOR and MAPK signaling pathways under taSMG.

7. ROS scavenging attenuates the mitochondrial dysfunction induced by taSMG

Under taSMG, ROS scavenger *N*-acetylcysteine (NAC) was

used to determine if the above mentioned phenomena could be suppressed. Then, it was observed that the mRNA level of NADPH oxidase family gene was not increased by treatment of NAC under taSMG conditions (Figure 18) [59]. Using RT-PCR (Figure 19A) and qRT-PCR (Figure 19B) [59], it was found that mRNA levels of ATPase and ATP synthase were not decreased under taSMG in the presence of NAC.

In addition, I confirmed that taSMG-induced autophagy was inhibited by NAC treatment. In the presence of NAC, I found that there were no changes in autophagy-related mRNA (Figure 20A and B) and protein levels, including the LC3-II/I ratio (Figure 20C and D) [59].

Therefore, it was concluded that taSMG-induced ROS generation, mitochondrial dysfunction and autophagy are defended in the presence of NAC.

8. Hypergravity conditions do not affect HL cell growth

In this study, microgravity was confirmed to have an anti-cancer effect, and conversely, I was curious about the growth of cancer cells under hypergravity conditions. Therefore, the experiment was conducted using the hypergravity controller provided by the Sungwan Kim team at Seoul National University (Figure 21A). After seeding in 1,000,000 cells/30 ml media in 25 cm^2 flask, and incubating for 24 hours under conditions of 1, 3, 5, 7, and 9 G, cell number was measured. Since only one gravity value can be set in the hypergravity controller, it was analyzed as a relative value for each 1 G condition. It was confirmed that there is no change in the HL cell even if the

gravity increases compared to 1 G (Figure 21B).

This section describes the operation of 3D clinostat and cell culture conditions in 3D clinostat. Under these conditions, taSMG inhibited cell number in human HL and breast cancer cells. taSMG caused ROS generation and mitochondrial dysfunction, and autophagy was induced through AMPK/Akt/mTOR and MAPK signaling. Treatment of NAC prevented the phenomenon caused by taSMG. It was confirmed that the taSMG did not affect cell number, ROS formation and mitochondrial mass. These results are covered in detail in the next section.

.

Figure 1. Microgravity laboratory at the ISS

The international space station (ISS) has a microgravity laboratory and is actively conducting a wide variety of studies, including changes in the human body due to microgravity [14-18].

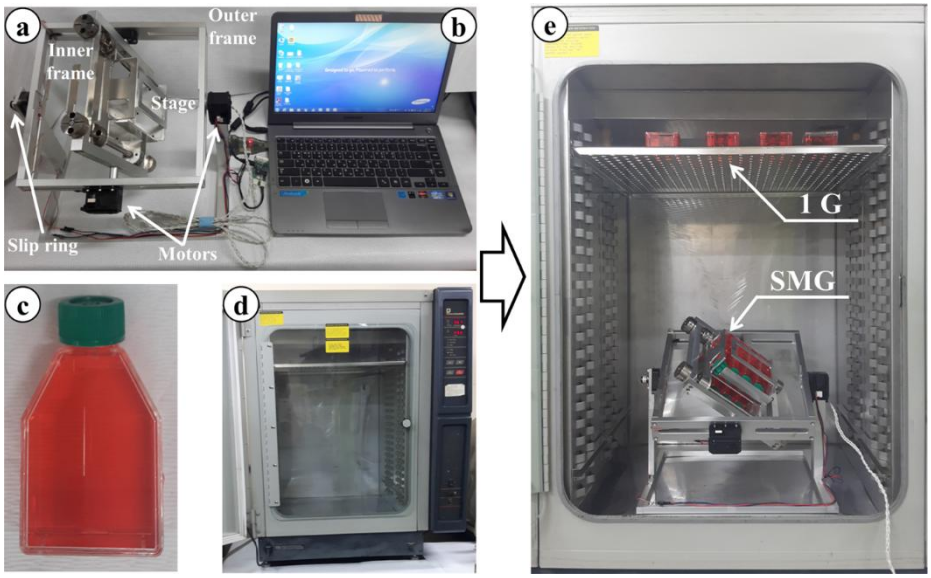

Figure 2. 3D clinostat design

(A) Three dimensional clinostat hardware. The hardware consists of two frames, outer frame and inner frame, with perpendicular rotational axes. The power and communication wires are connected via the slip ring. (B) PC for control, (C) 25 cm^2 flask for cell proliferation, (D) incubator, (E) experimental set-up [58].

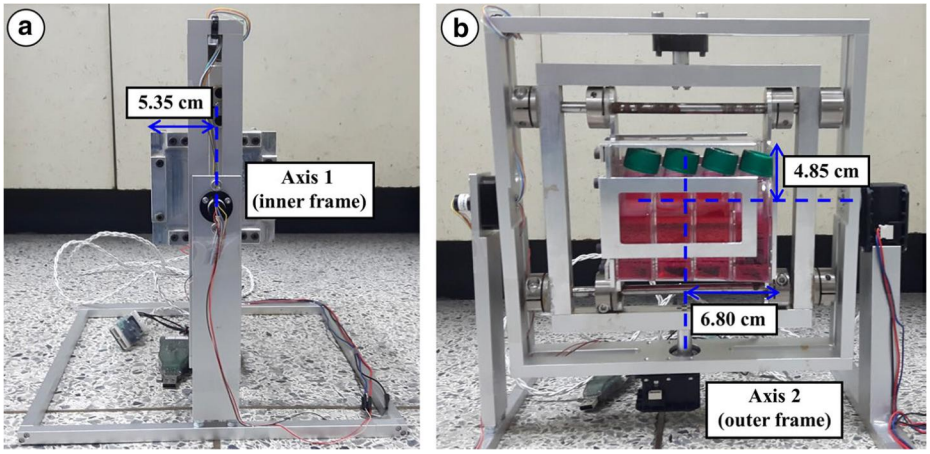

Figure 3. The quantitative dimensions of the mechanical stage relative to its center of rotation

Dimension of stage for flasks. (A) left side, (B) front side [58].

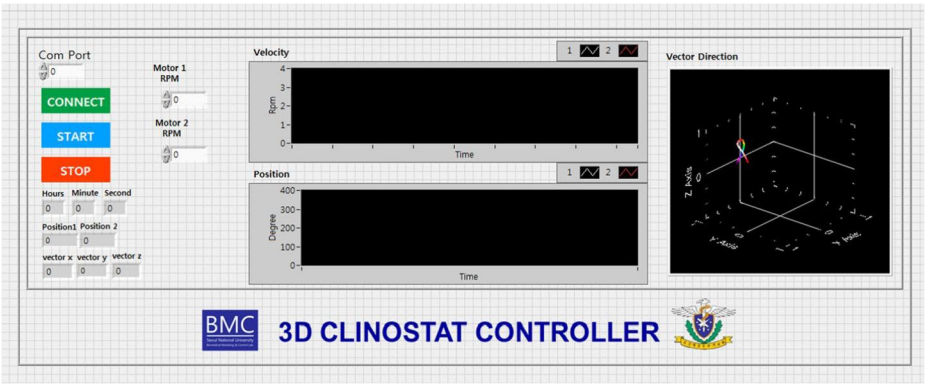

Figure 4. The optimal angular velocities were determined according to simulation based on the kinematic model

A graphical user interface was implemented using LabVIEW-based graphic user interface for control of 3D clinostat [58].

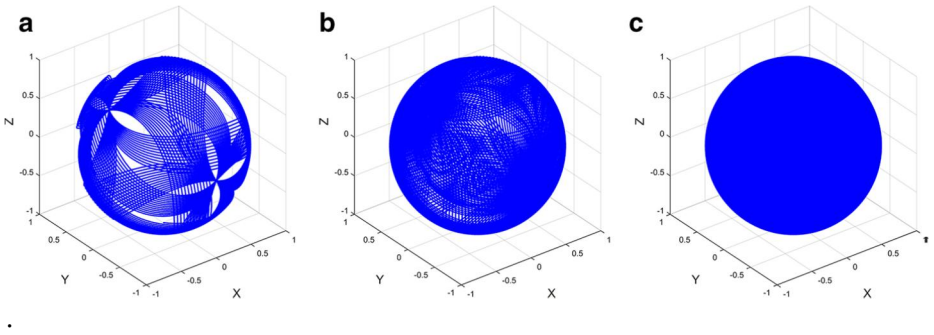

Figure 5. The combination of the two angular velocities showed symmetric acceleration distribution

Acceleration distribution of 3D clinostat with optimized angular velocities (outer frame: 0.913 rpm, inner frame: 0.683 rpm); acceleration distribution after (A) 1 h, (B) 2 h, and (C) 3 h [58].

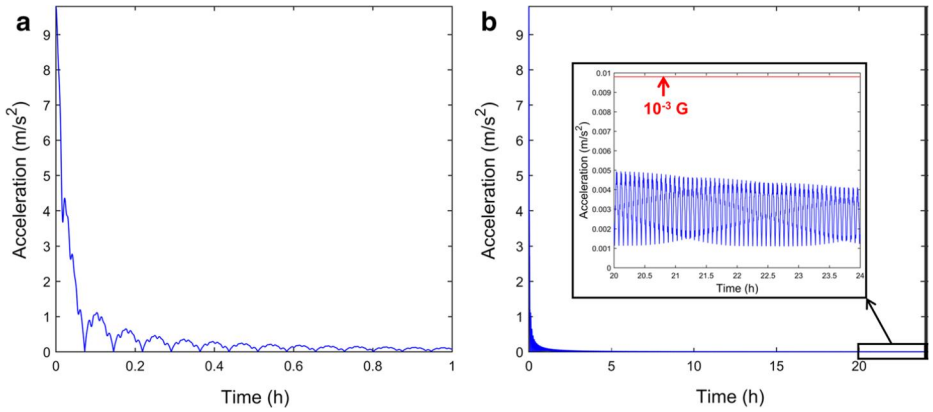

Figure 6. The gravitational, centrifugal, and tangential accelerations were considered in calculation of time-averaged simulated microgravity.

(A) Time-averaged acceleration from 0 to 1 h, (B) Time-averaged acceleration from 0 to 24 h. The location of analysis is $[\Delta x\ \Delta y\ \Delta z] = [0.1\ m\ 0.1\ m\ 0.1\ m]$ from the center of the clinostat. The acceleration is smaller than 10^{-3} G when reached 24 h [58].

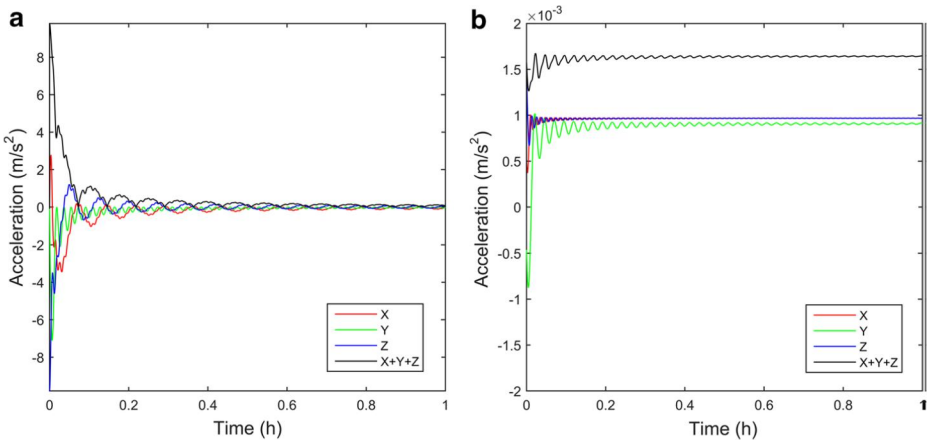

Figure 7. Time-averaged gravitational and non-gravitational acceleration

The acceleration consists of (A) gravitational acceleration and (B) non-gravitational acceleration. The gravitational acceleration decreases continuously whereas the non-gravitational acceleration does not asymptote to zero [58].

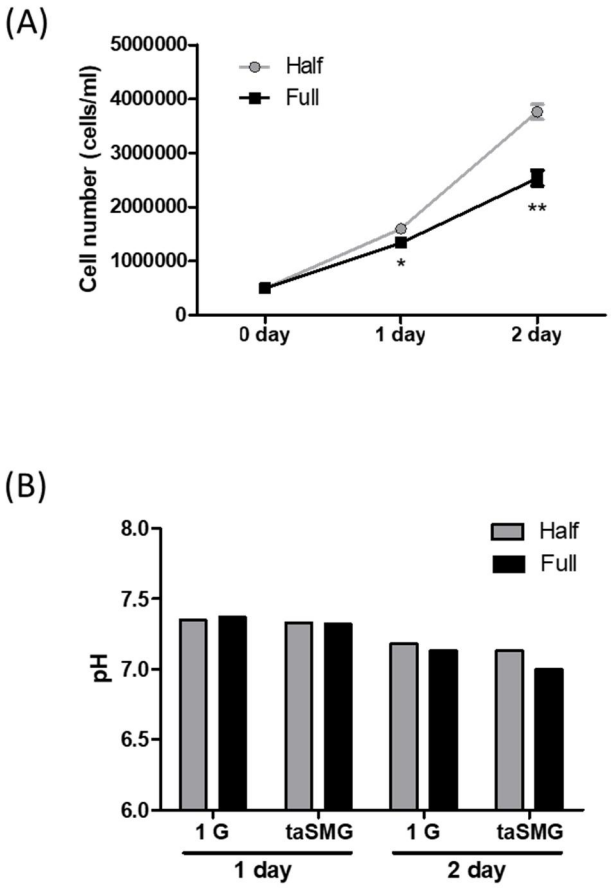

Figure 8. In 3D clinostat culture system, conditions may be different from general culture system

Human HL cell line L-540 cells were cultured under half- and full-filled media condition from 1 to 2 days. (A) Cell number of L-540. (B) pH measurement of media after incubation in half- and full-filled media condition Data are presented as mean ± SEM; $^{*}p < 0.05$ and $^{**}p < 0.005$ vs. the half-filled media group.

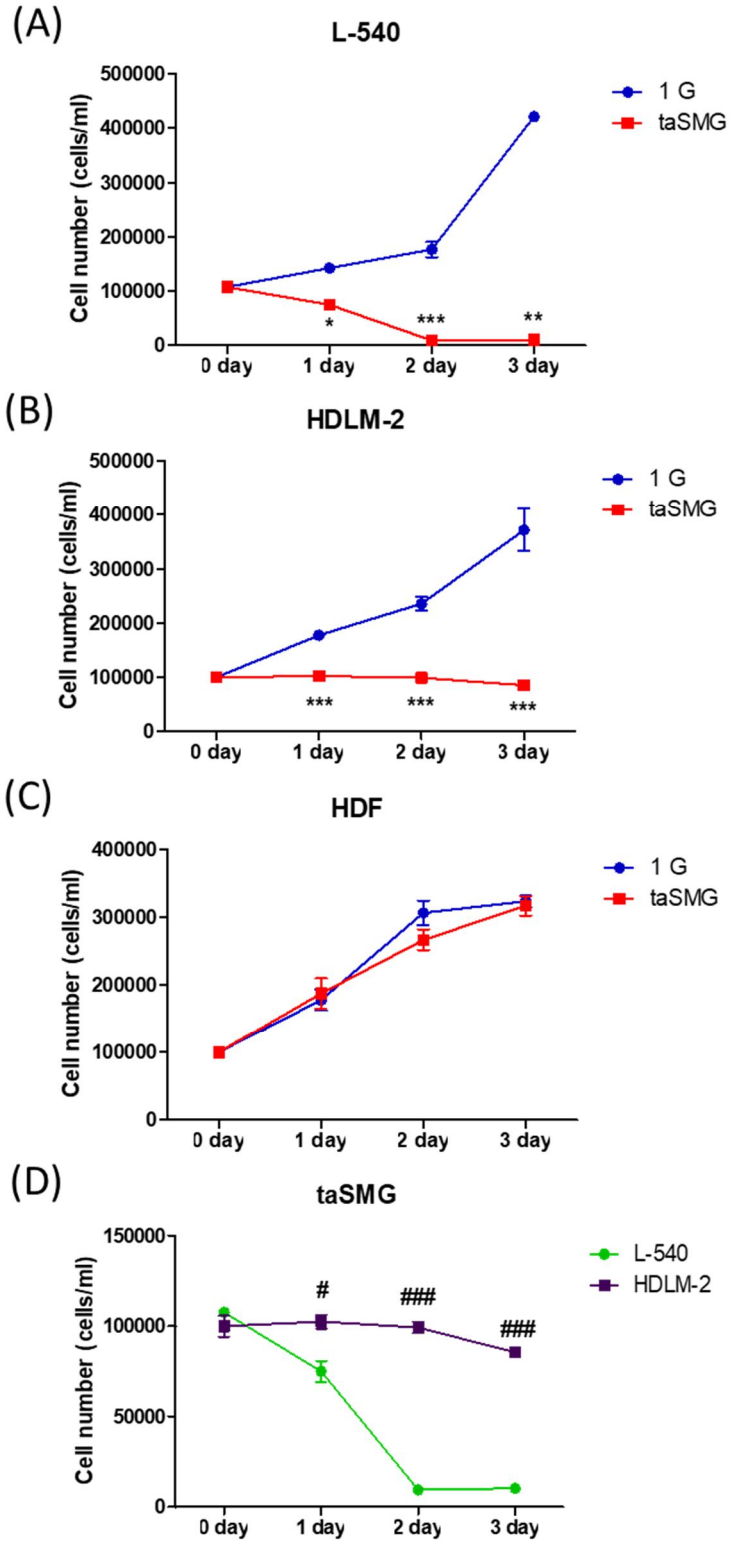
(A)
L-540
Cell number (cells/ml)
500000
400000
300000
200000
100000
0
0 day
1 day
2 day
3 day
*
***
**
1 G
taSMG
(B)
HDLM-2
Cell number (cells/ml)
500000
400000
300000
200000
100000
0
0 day
1 day
2 day
3 day
***
***
***
1 G
taSMG
(C)
HDF
Cell number (cells/ml)
400000
300000
200000
100000
0
0 day
1 day
2 day
3 day
1 G
taSMG
(D)
taSMG
Cell number (cells/ml)
150000
100000
50000
0
0 day
1 day
2 day
3 day
#
###
###
L-540
HDLM-2

Figure 9. Effect of time-averaged simulated microgravity on cell growth

Human HL cell lines, (A) L-540 and (B) HDLM-2, and (C) normal human dermal fibroblast (HDF) cells were cultured under 1 G or taSMG from 1 to 3 days. (D) Cell proliferation of L-540 cell was compared with that of HDLM-2 cells under taSMG. Data are presented as mean ± SEM; $^{*}p < 0.05$, $^{**}p < 0.005$, and $^{***}p < 0.0005$ vs. the 1 G control group. $^{\#}p < 0.05$ and $^{\#\#\#}p < 0.0001$ vs. the L-540 group [58].

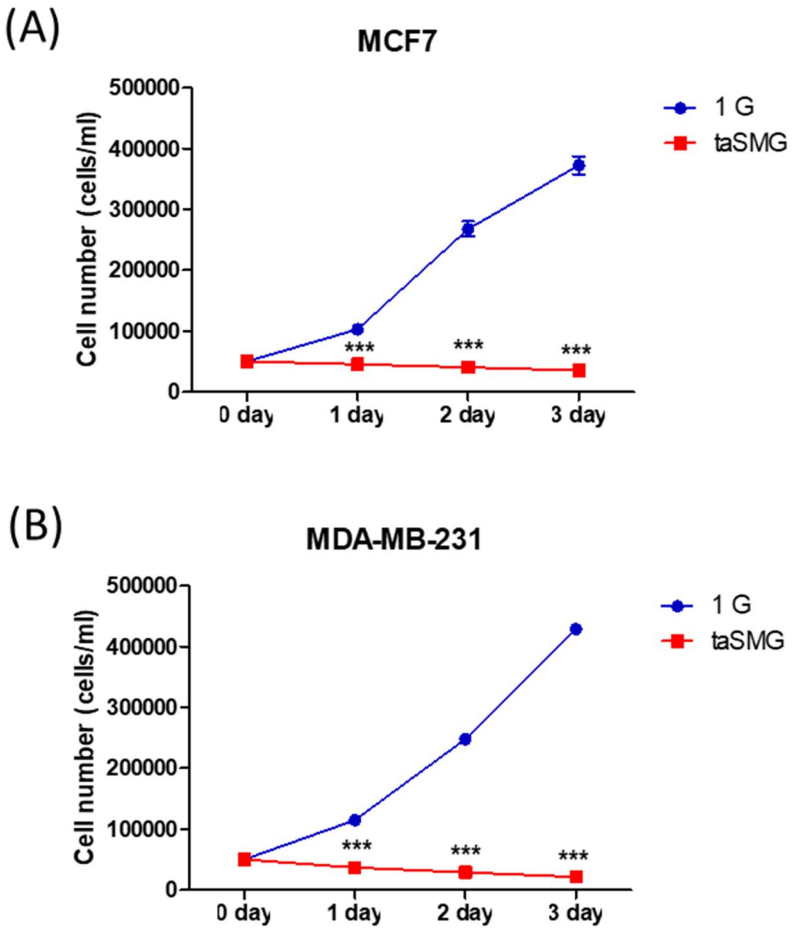

Figure 10. Time-averaged simulated microgravity also inhibits the growth of adherent cancer cells

Human breast cancer cell lines, (A) MCF7 and (B) MDA-MB-231 cells were cultured under 1 G or taSMG from 1 to 3 days. Data are presented as mean ± SEM; $^{*}p < 0.05$, $^{**}p < 0.005$, and $^{***}p < 0.0005$ vs. the 1 G control group.

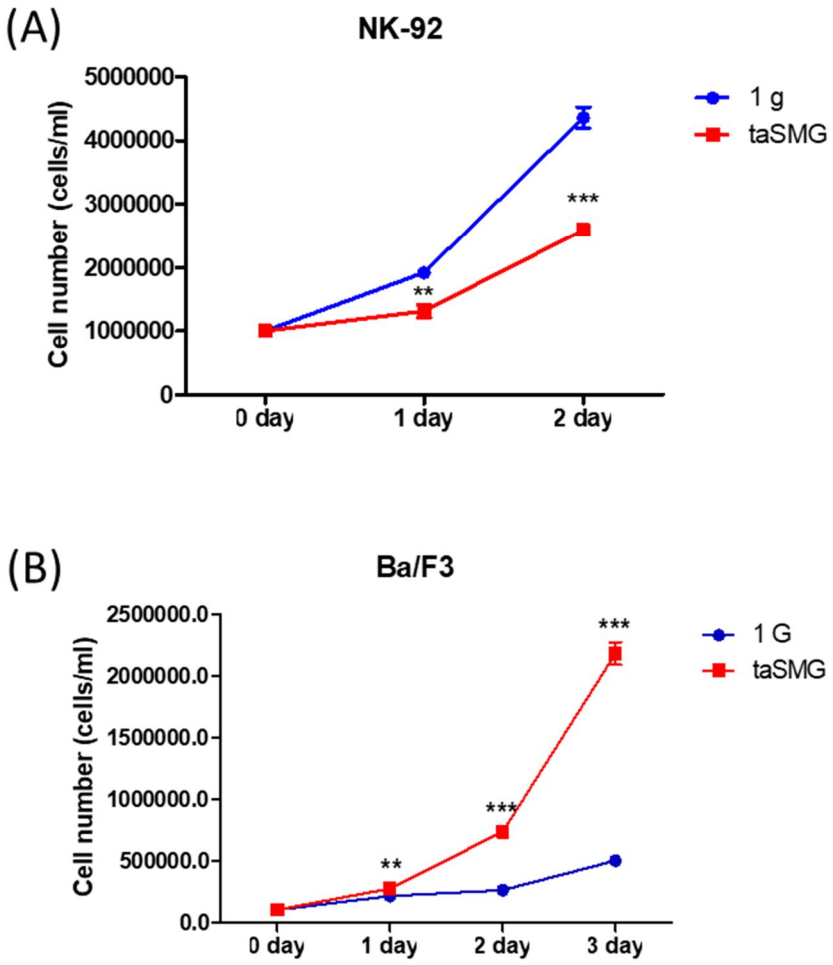

Figure 11. The cell growth of immune cell line in time-averaged simulated microgravity.

The growth of (A) human NK cell line, NK-92 cells (B) murine pro-B cell line, Ba/F3 cells under 1 G or taSMG from 1 to 3 days. Data are presented as mean ± SEM; $^{**}p < 0.005$, and $^{***}p < 0.0005$ vs. the 1 G control group.

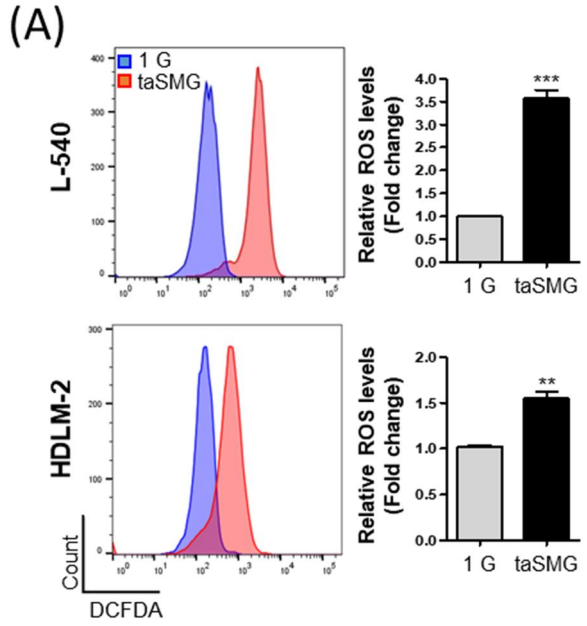
(A)
L-540
1 G
taSMG
Relative ROS levels (Fold change)
***
1 G
taSMG
HDLM-2
**
Count
DCFDA

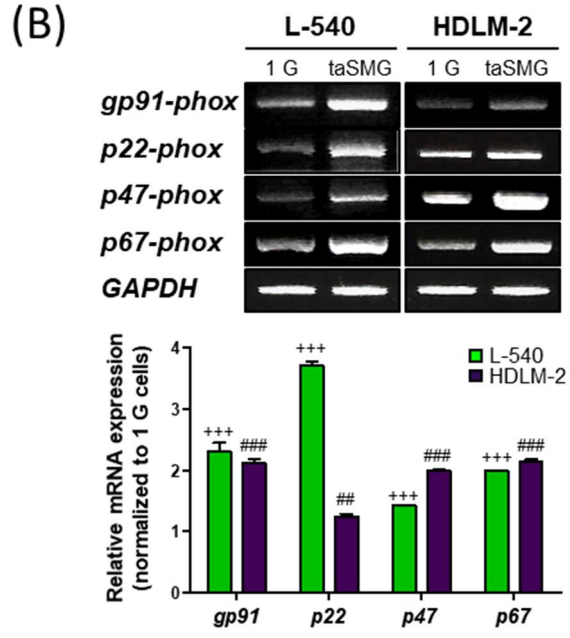
(B)
L-540
HDLM-2
1 G
taSMG
gp91-phox
p22-phox
p47-phox
p67-phox
GAPDH
Relative mRNA expression (normalized to 1 G cells)
L-540
HDLM-2
gp91
p22
p47
p67

Figure 12. Time-averaged simulated microgravity increases ROS generation and expression of NADPH oxidase family genes in human HL cells.

Human HL cell lines (L-540 and HDLM-2) incubated in 1 G or taSMG conditions for 2 days were harvested. (A) ROS generation was determined by 2',7'-dichlorofluorescin diacetate (DCFDA) staining. (B) RT-PCR analysis of NADPH oxidase family genes (*gp91-*, *p22-*, *p47-*, and *p67-phox*). Data represent the mean ± SEM, n = 4. $^{**}p < 0.01$ and $^{***}p < 0.001$ vs. the 1 G group. $^{+++}p < 0.0001$ vs. the 1 G group of L-540 cells. $^{\#\#}p < 0.01$ and $^{\#\#\#}p < 0.001$ vs. the 1 G group of HDLM-2 cells. 1 G: normal gravity conditions; taSMG: time-averaged simulated microgravity [59].

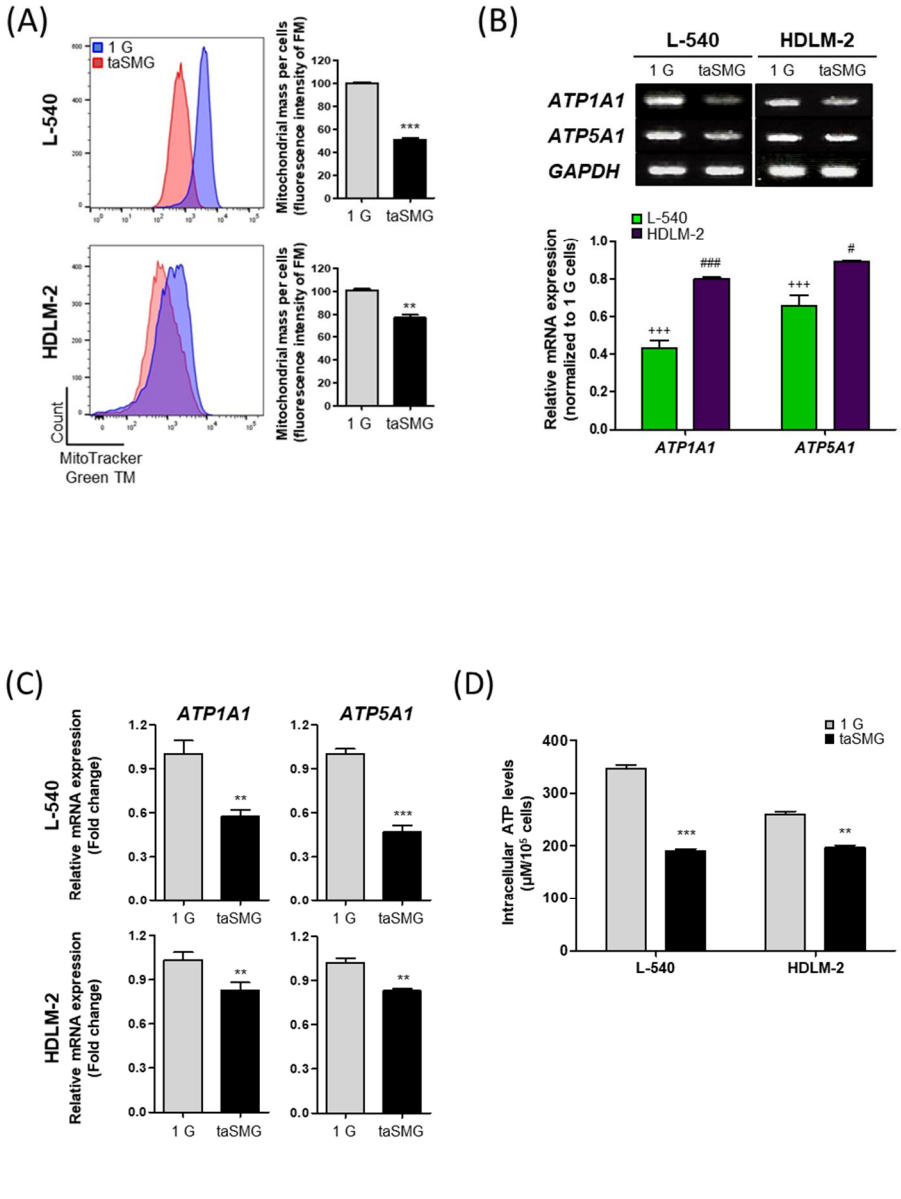
(A)
L-540
HDLM-2
1 G
taSMG
Count
MitoTracker Green TM
Mitochondrial mass per cells (fluorescence intensity of FM)
***
**
(B)
L-540
HDLM-2
1 G
taSMG
ATP1A1
ATP5A1
GAPDH
Relative mRNA expression (normalized to 1 G cells)
+++
###
#
(C)
ATP1A1
ATP5A1
Relative mRNA expression (Fold change)
(D)
Intracellular ATP levels (μM/10^5 cells)

Figure 13. Time-averaged simulated microgravity induces mitochondrial dysfunction in human HL cells.

Human HL cell lines (L-540 and HDLM-2) incubated in 1 G or taSMG conditions for 2 days were harvested. (A) Mitochondrial mass was analyzed by MitoTracker Green FM. (B) RT-PCR and (C) qRT-PCR analysis of ATPase (*ATP1A1*) and ATP synthase (*ATP5A1*) mRNA levels. (D) Analysis of intracellular ATP levels in HL cells. Data represent the mean ± SEM, n = 4. $^{**}p <$ 0.01 and $^{***}p < 0.001$ vs. the 1 G group. $^{+++}p < 0.0001$ vs. the 1 G group of L-540 cells. $^{\#}p < 0.05$, $^{\#\#}p < 0.01$ and $^{\#\#\#}p < 0.001$ vs. the 1 G group of HDLM-2 cells. The grouping of gels cropped from different gels. 1 G: normal gravity conditions; taSMG: time-averaged simulated microgravity [59].

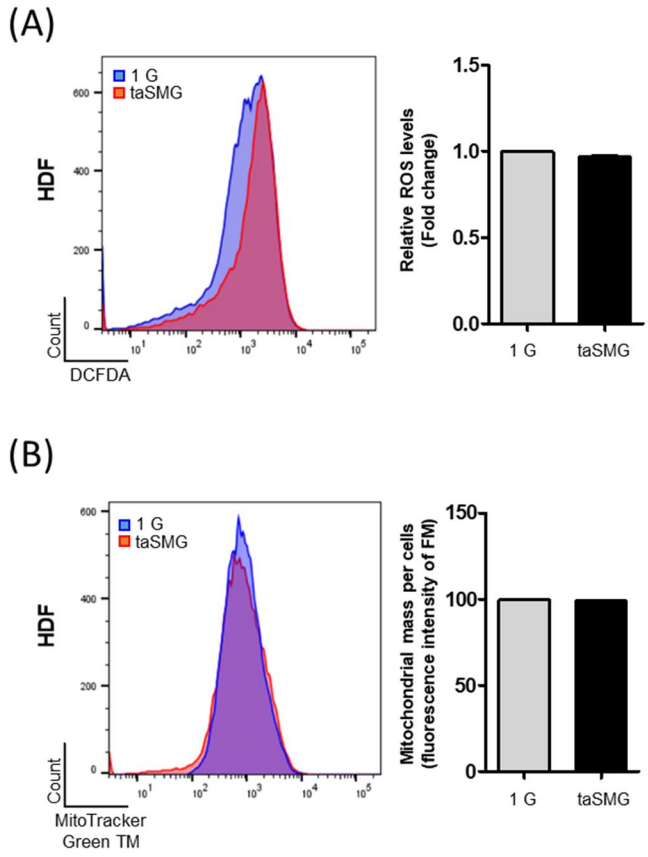

Figure 14. Time-averaged simulated microgravity does not affect ROS generation and mitochondrial mass in normal HDF cells.

Normal HDF cells incubated in 1 G or taSMG conditions for 2 days were harvested. (A) ROS generation was determined by 2',7'-dichlorofluorescin diacetate (DCFDA) staining. (B) Mitochondrial mass was analyzed by MitoTracker Green FM. 1 G: normal gravity conditions; taSMG: time-averaged simulated microgravity.

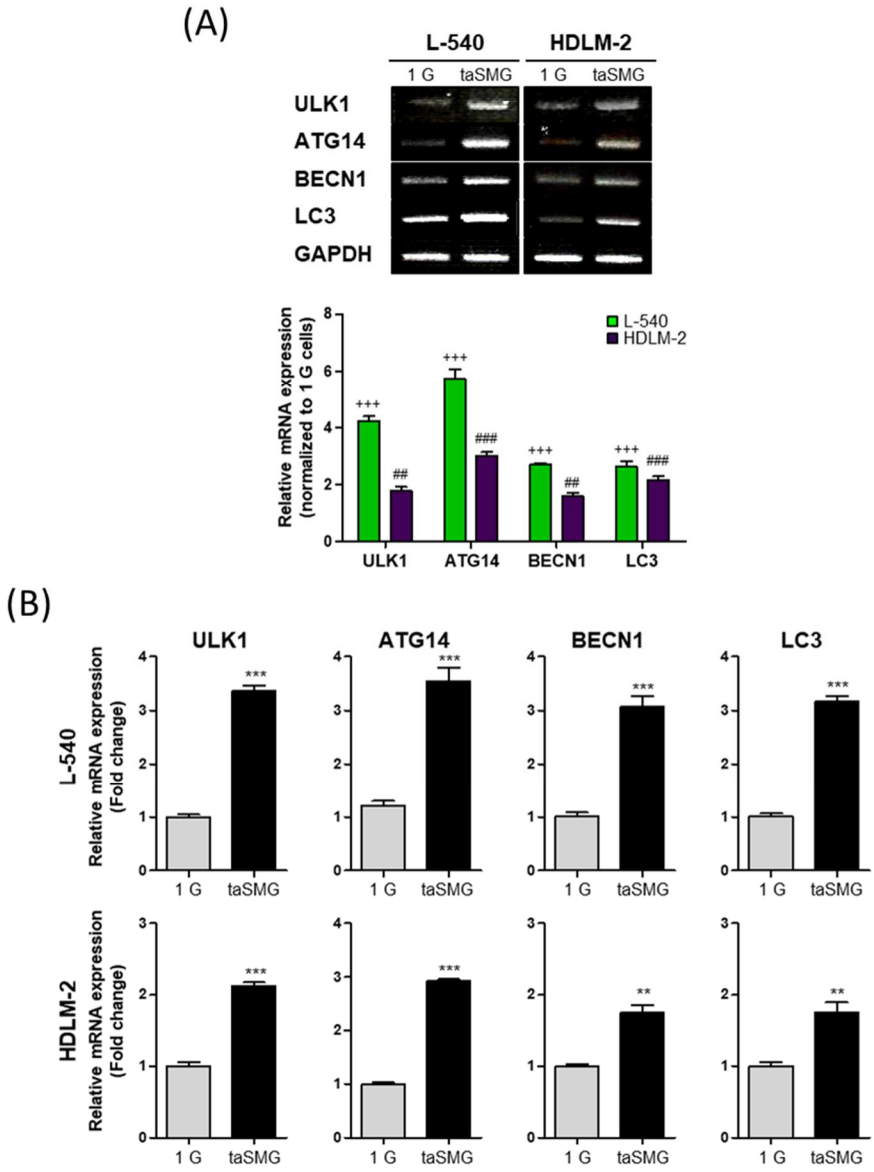
(A)
L-540
HDLM-2
1 G
taSMG
1 G
taSMG
ULK1
ATG14
BECN1
LC3
GAPDH
Relative mRNA expression
(normalized to 1 G cells)
L-540
HDLM-2
+++
##
+++
###
+++
##
+++
###
ULK1
ATG14
BECN1
LC3
(B)
ULK1
ATG14
BECN1
LC3
L-540
HDLM-2
Relative mRNA expression
(Fold change)
***
**
1 G
taSMG

(C)

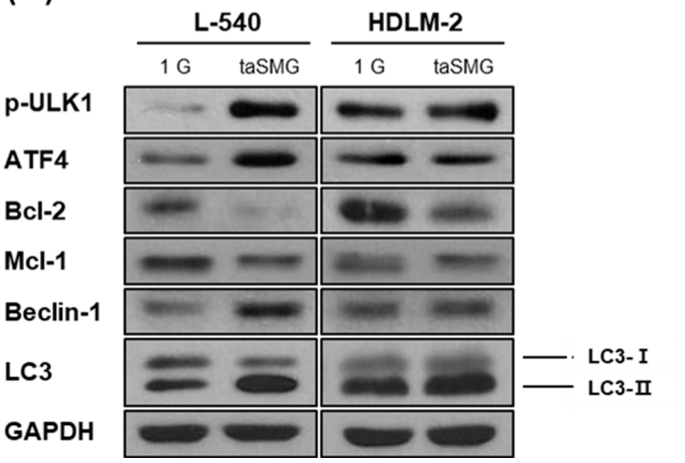
L-540
HDLM-2
1 G
taSMG
1 G
taSMG
p-ULK1
ATF4
Bcl-2
Mcl-1
Beclin-1
LC3
GAPDH
LC3-Ⅰ
LC3-Ⅱ

(D)

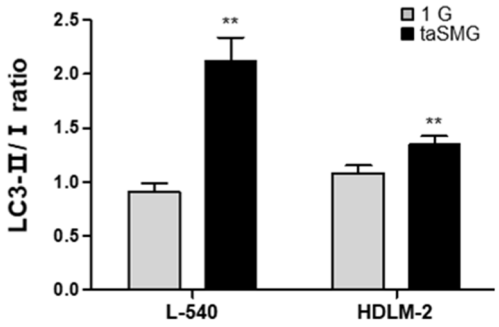
LC3-Ⅱ/Ⅰ ratio
2.5
2.0
1.5
1.0
0.5
0.0
**
**
1 G
taSMG
L-540
HDLM-2

Figure 15. Time-averaged simulated microgravity contributes to induce autophagy

(A) RT-PCR and (B) qRT-PCR analysis of mRNA levels of autophagy-related genes. (C) Western blot analysis of autophagy-related proteins. GAPDH was used as the loading control. Densitometric analysis of protein expression was determined after normalization to GAPDH. The red dotted line indicates the base line. (D) Densitometric analysis of the LC3-II/I ratio was determined after normalization to GAPDH. Data represent the mean ± SEM, n = 4. $^{+++}p < 0.0001$ vs. the 1 G group of L-540 cells. $^{\#}p < 0.05$, $^{\#\#}p < 0.01$ and $^{\#\#\#}p < 0.001$ vs. the 1 G group of HDLM-2 cells. $^{**}p < 0.01$ and $^{***}p < 0.001$ vs. the 1 G group. The grouping of gels and blots cropped from different gels. 1 G: normal gravity conditions; taSMG: time-averaged simulated microgravity [59].

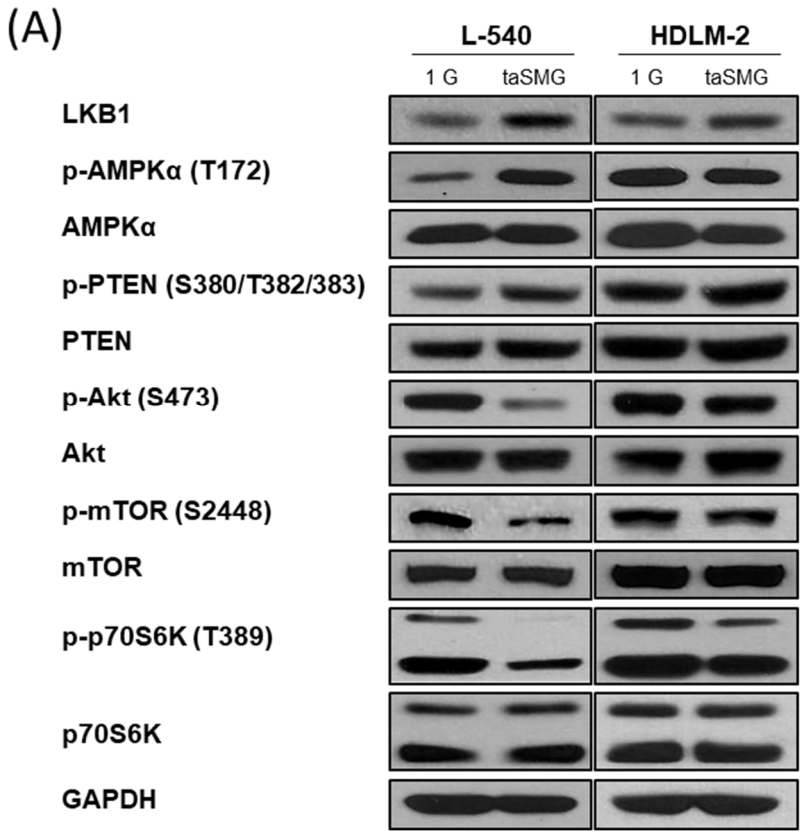
(A)
L-540
HDLM-2
1 G
taSMG
1 G
taSMG
LKB1
p-AMPKα (T172)
AMPKα
p-PTEN (S380/T382/383)
PTEN
p-Akt (S473)
Akt
p-mTOR (S2448)
mTOR
p-p70S6K (T389)
p70S6K
GAPDH

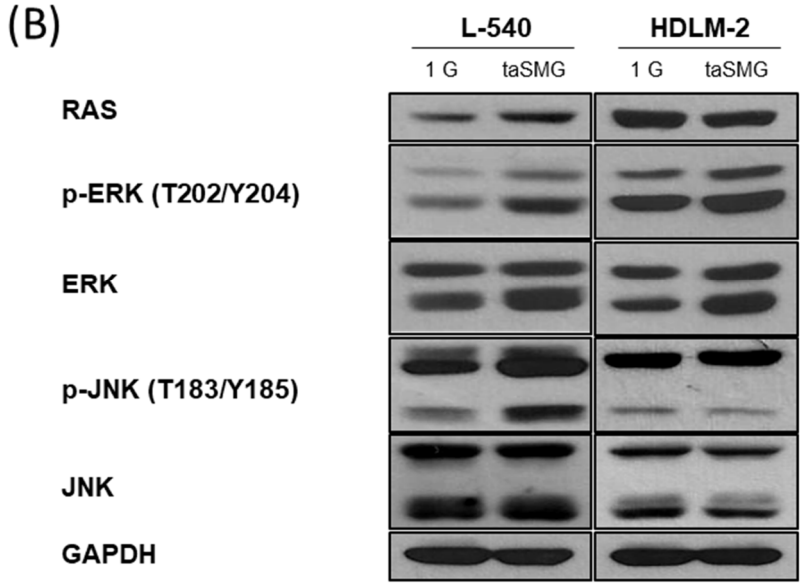
(B)
L-540
HDLM-2
1 G
taSMG
1 G
taSMG
RAS
p-ERK (T202/Y204)
ERK
p-JNK (T183/Y185)
JNK
GAPDH

Figure 16. The regulation of AMPK/Akt/mTOR and MAPK pathways under time-averaged simulated microgravity in human HL cells

(A) Representative blots showing the phosphorylation levels of AMPK, PTEN, Akt, mTOR and S6K and total levels of LKB1, AMPK, PTEN, Akt, mTOR, and S6K in HL cells were determined by Western blotting. (B) Representative blots showing the activation levels of the MAPK pathway components RAS, ERK and JNK. All experiments were performed at least in quadruplicate. The grouping of gels cropped from different blots. 1 G: normal gravity conditions; taSMG: time-averaged simulated microgravity [59].

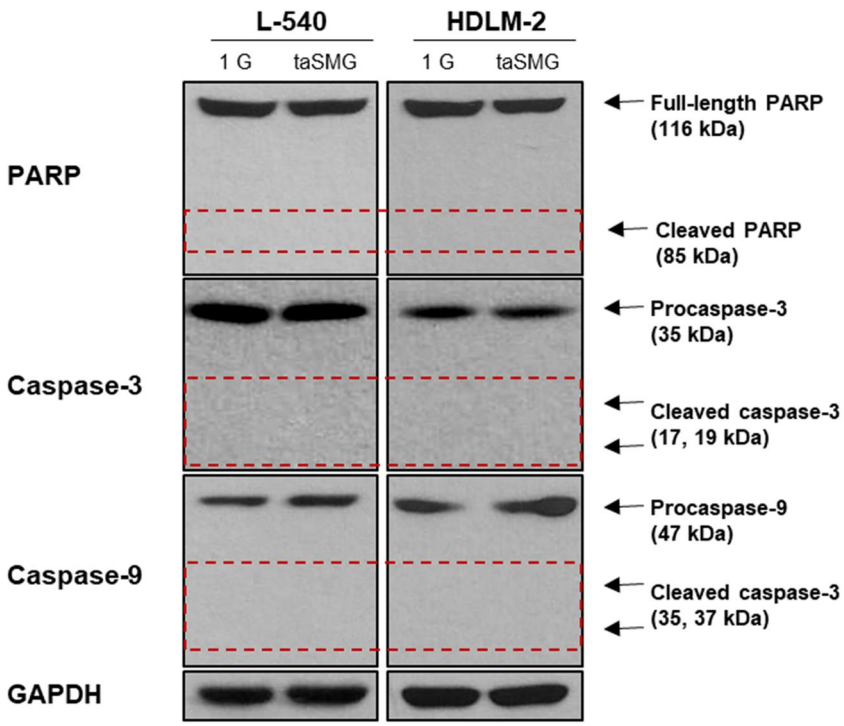

Figure 17. Time-averaged simulated microgravity does not induce apoptosis in human HL cells

Representative blots showing apoptosis markers (PARP, caspase-3 and caspase-9). The dashed line is cleaved size that indicates apoptosis activation. All experiments were performed at least in quadruplicate. The grouping of gels cropped from different blots. 1 G: normal gravity conditions; taSMG: time-averaged simulated microgravity [59].

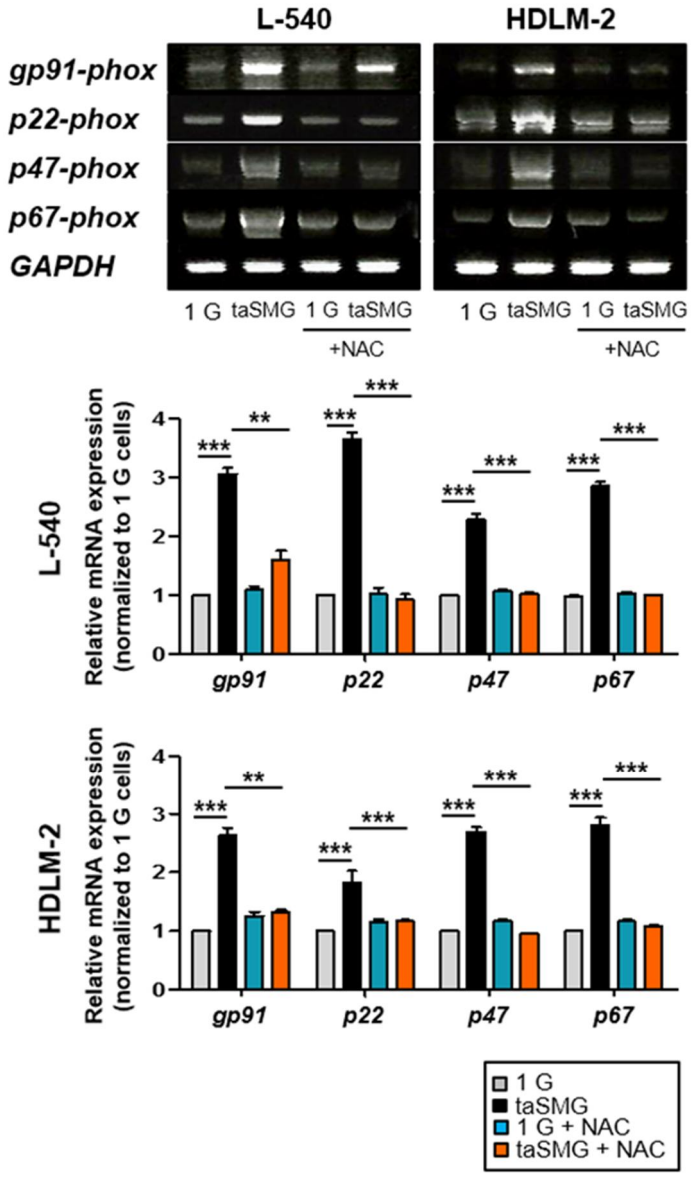
L-540
HDLM-2
gp91-phox
p22-phox
p47-phox
p67-phox
GAPDH
1 G taSMG 1 G taSMG
+NAC
1 G taSMG 1 G taSMG
+NAC
L-540
HDLM-2
Relative mRNA expression
(normalized to 1 G cells)
gp91
p22
p47
p67
1 G
taSMG
1 G + NAC
taSMG + NAC

Figure 18. *N*-acetylcysteine prevents increased expression of the NADPH oxidase family genes by time-averaged simulated microgravity in human HL cells

RT-PCR data shows the mRNA levels of NADPH oxidase family genes. Data represent the mean ± SEM, n = 4. $^{**}p < 0.01$ and $^{***}p < 0.001$ vs. the 1 G group or taSMG. The grouping of gels cropped from different blots. 1 G: normal gravity conditions; taSMG: time-averaged simulated microgravity. Treatment of NAC proceeded under the same conditions [59].

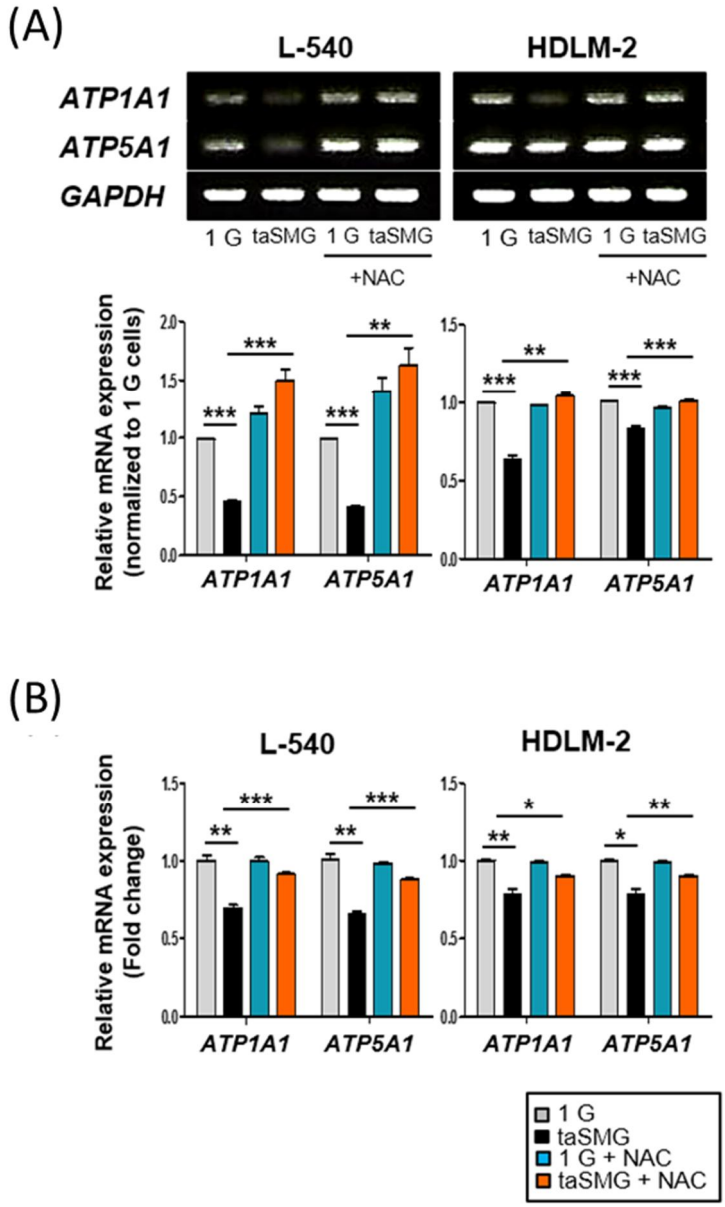
(A)
L-540
HDLM-2
ATP1A1
ATP5A1
GAPDH
1 G taSMG 1 G taSMG
+NAC
1 G taSMG 1 G taSMG
+NAC
Relative mRNA expression
(normalized to 1 G cells)
ATP1A1
ATP5A1
ATP1A1
ATP5A1
(B)
L-540
HDLM-2
Relative mRNA expression
(Fold change)
ATP1A1
ATP5A1
ATP1A1
ATP5A1
1 G
taSMG
1 G + NAC
taSMG + NAC

Figure 19. *N*-acetylcysteine protects mitochondrial dysfunction by time-averaged simulated microgravity in human HL cells

(A) RT-PCR and (B) qRT-PCR analysis of mRNA levels of ATPase and ATP synthase. Data represent the mean ± SEM, n = 4. $^{*}p < 0.05$, $^{**}p < 0.01$ and $^{***}p < 0.001$ vs. the 1 G group or taSMG. The grouping of gels cropped from different blots. 1 G: normal gravity conditions; taSMG: time-averaged simulated microgravity. Treatment of NAC proceeded under the same conditions [59].

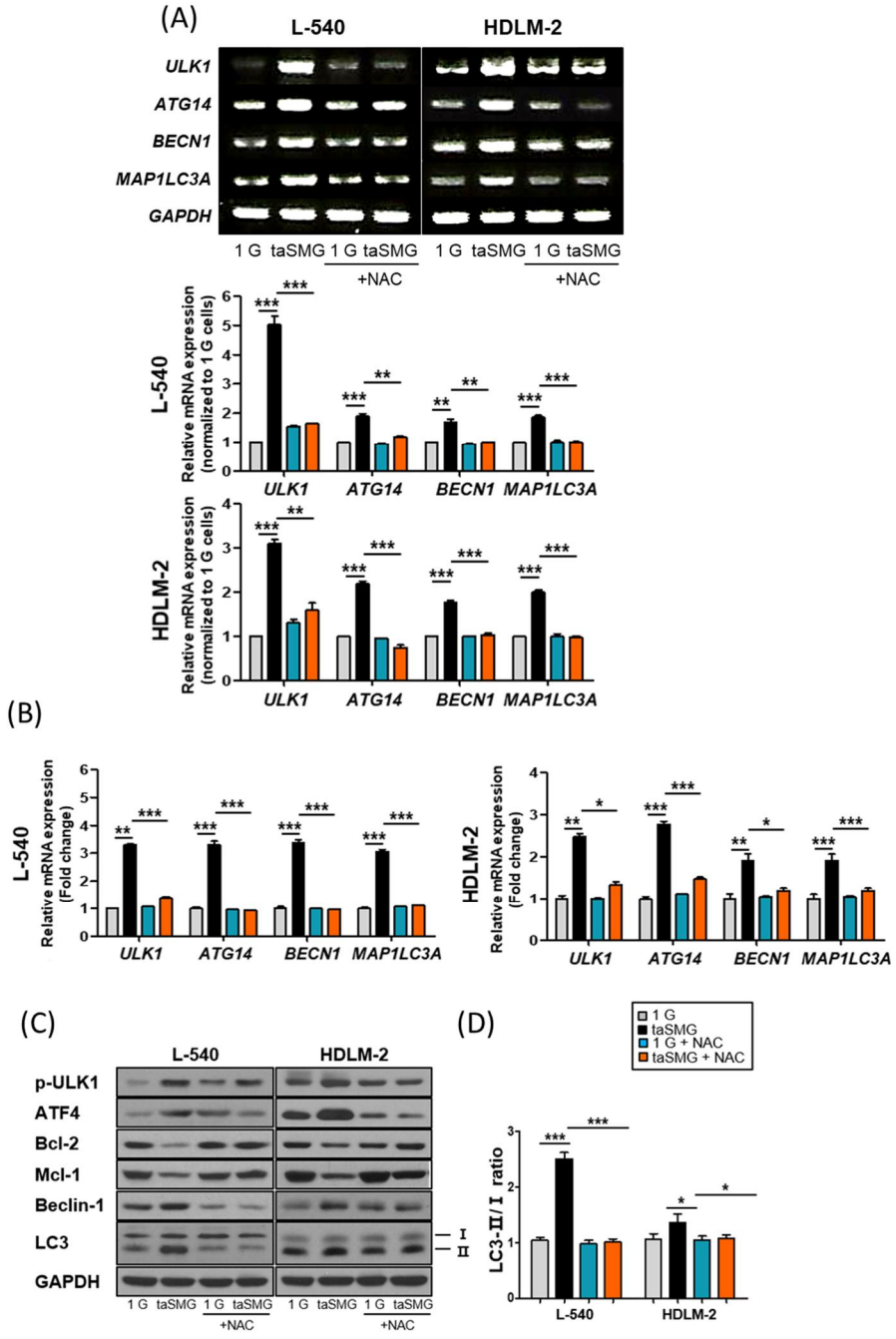
(A)
L-540
HDLM-2
ULK1
ATG14
BECN1
MAP1LC3A
GAPDH
1 G taSMG 1 G taSMG 1 G taSMG 1 G taSMG
+NAC
+NAC
L-540
HDLM-2
Relative mRNA expression (normalized to 1 G cells)
ULK1 ATG14 BECN1 MAP1LC3A
(B)
L-540
HDLM-2
Relative mRNA expression (Fold change)
ULK1 ATG14 BECN1 MAP1LC3A
(C)
L-540
HDLM-2
p-ULK1
ATF4
Bcl-2
Mcl-1
Beclin-1
LC3
GAPDH
I
II
1 G taSMG 1 G taSMG 1 G taSMG 1 G taSMG
+NAC
+NAC
(D)
1 G
taSMG
1 G + NAC
taSMG + NAC
LC3-II/I ratio
L-540
HDLM-2

Figure 20. N-acetylcysteine prevents autophagy by time-averaged simulated microgravity

(A) RT-PCR and (B) qRT-PCR shows mRNA levels of autophagy-related genes. (C) Western blot analysis of protein levels of autophagy-related genes. (D) Densitometric analysis of LC3-II/I ratio was determined after normalization to GAPDH. Data represent the mean ± SEM, n = 4. $*p < 0.05$, $**p < 0.01$ and $***p < 0.001$ vs. the 1 G group or taSMG. The grouping of gels cropped from different blots. 1 G: normal gravity conditions; taSMG: time-averaged simulated microgravity. Treatment of NAC proceeded under the same conditions [59].

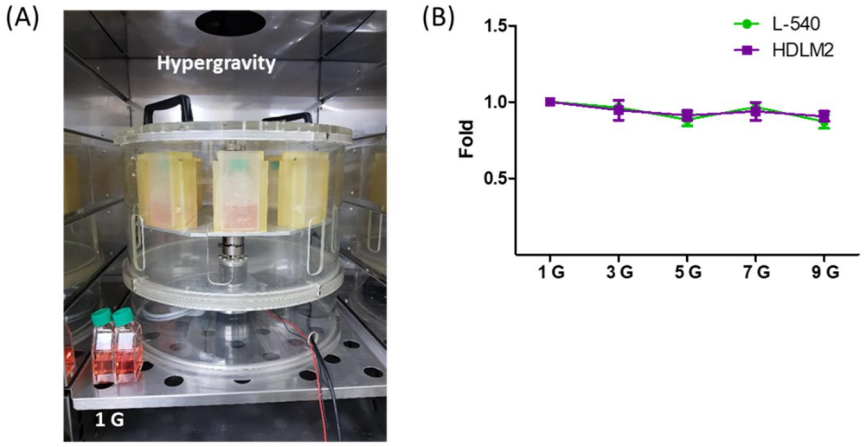

Figure 21. The growth of human HL cells was unchanged under hypergravity condition

(A) The experiment was conducted using the hypergravity controller provided by the Sungwan Kim team at Seoul National University. (B) After incubating for 24 hours under conditions of 1, 3, 5, 7, and 9 G, cell number was measured. Since only one gravity value can be set in the hypergravity controller, it was analyzed as a relative value for each 1 G condition. Data represent the mean ± SEM, n = 4

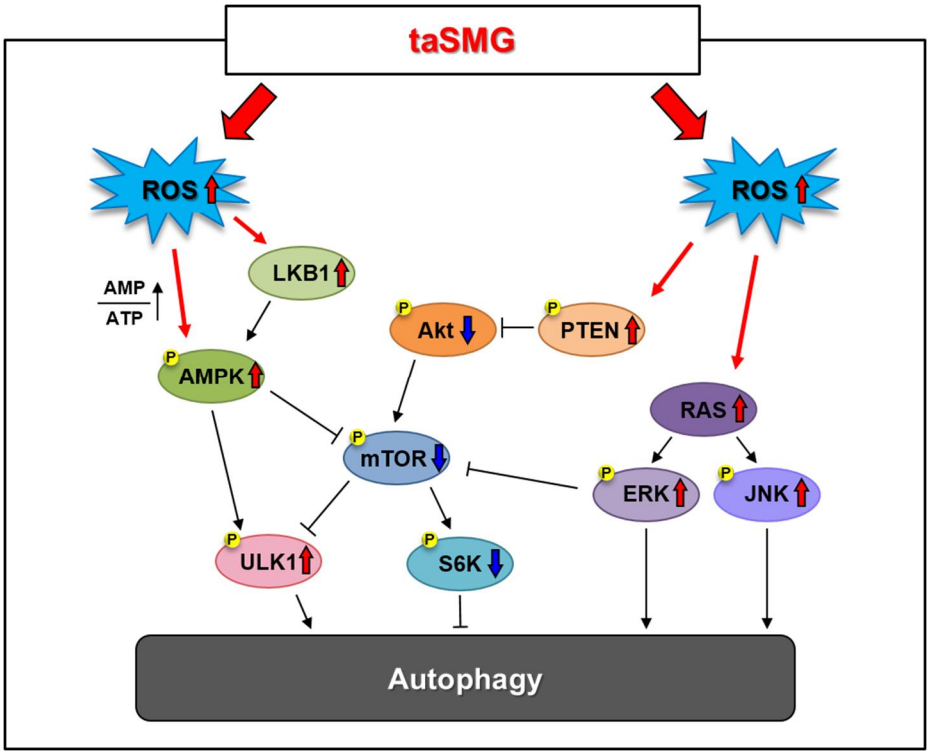

Figure 22. Schematic representation of the time-averaged simulated microgravity-induced autophagy mechanism in human Hodgkin's lymphoma cells

taSMG induces the activation of AMPK, PTEN, and MAPK, and as well as the suppression of Akt, leading to the inhibition of mTOR activity. The downstream regulator S6K, which inhibits autophagy, is consequently suppressed, resulting in autophagy in human HL cells [59].

DISCUSSION

The present 3D clinostat with optimized angular velocities was tested for its nullification of gravity vector without repeated trajectory using kinematics model based simulation. The time-averaged acceleration was gradually decreased, and reached 1.7 × 10^{-4} G after 24 h of operation. Compared with previous studies [79], the present results indicate that sufficient time-averaged acceleration was provided with symmetric acceleration distribution. The time-averaged acceleration did not asymptote to zero-gravity as centrifugal acceleration was applied to radial direction continuously and therefore not cancelled. However, the centrifugal acceleration is proportional to the square of the angular velocity, and the angular velocities provided in this study were sufficiently small (0.913 and 0.683 rpm). In order to minimize the residual acceleration of the 3D clinostat and assume quasi-static state, operation with minimum angular velocities is required. However, this may result in the taSMG generated not being recognized by cells, as a consequence of the extremely slow change in orientation.

Primary chemo-, radio-therapy results in cure rates of 90% and 80% in HL patients with early- and advanced-stage disease, respectively [80]. However, these treatments lead to a significant risk of short- and long-term toxicities, which can also cause secondary malignancies [81, 82]. Therefore, new therapies based on suppressing disease progression mechanisms, including molecule-specific inhibition are needed for successful

treatment.

As taSMG can be achieved artificially, studies using this technique have advanced rapidly. Based on symptoms experienced by astronauts in the space such as muscle atrophy, bone loss, and immunodeficiency, microgravity has been investigated in the treatment of various diseases [2, 4, 6, 7, 20, 29]. In this study, I designed a clinostat that uses a specific algorithm aimed at randomizing the gravitational vector pattern and achieving a nullified time-averaged vector [58].

Microgravity in space has been reported to cause oxidative stress such as ROS production [83-85]. However, the study of microgravity induced oxidative stress is not yet fully understood. In this study, I validated my hypothesis that taSMG induces oxidative cellular stress in human HL cells, as demonstrated by elevated ROS and impaired mitochondrial function.

NADPH oxidase-dependent ROS production is implicated in many physiologic and pathophysiologic processes. NADPH oxidase mediated ROS can alter parameters of signal transduction, mitochondrial damage, cell proliferation, cell death and autophagy [34, 35, 69, 85]. I also found that taSMG upregulates NADPH oxidase family genes while decreasing the mitochondrial mass, and lowering ATPase, and ATP synthase levels, resulting in reduced intracellular ATP levels [59].

Autophagy mediates the bulk degradation of intracellular through lysosomal-dependent mechanisms and is necessary for the maintenance of cellular homeostasis [31, 32, 34]. Autophagy is also induced in response to oxidative stress caused by ROS and RNS [34-36]. In fact, the role of autophagy in cancer

remains controversial given that it varies according to the type of cancer. Autophagy may contribute to cancer progression by increasing cell migration and invasion; conversely, it can have an anticancer effect by decreasing cell proliferation, and promoting cancer cell death [39, 42, 45–47]. I hypothesized that autophagy would occur due to increased ROS, and interestingly, autophagy was induced under taSMG [59].

Recently, some research reported that autophagy is induced in simulated microgravity and inhibits cancer proliferation and metastasis [30, 33, 86]. However, its molecular mechanisms are unclear yet. As an intracellular energy sensor, AMPK signaling serves as a mitochondrial function regulator to maintain energy homeostasis [40]. And recent studies have found that activation of AMPK results in autophagy through negative regulation of mTOR and phosphorylation of ULK1 [38–41]. Interestingly, it was confirmed that the mitochondrial dysfunction produced by taSMG promotes autophagy through modulation of the AMPK/Akt/mTOR and MAPK signaling pathways (Figure 22). Overall, the effect of taSMG was more prominent in L–540 cells than in HDLM–2 cells.

When culturing cells in 3D clinostat, I care a lot to ensure that the cells are not subjected to any stress other than taSMG. 1) The 3D clinostat machine should operate in the cell incubator in the same way as the original cell culture conditions. 2) Consider filling the media to rule out shearing flow stress caused by media flow due to clinostat rotation. 3) When the culture flask is filled with media is full, there must be sufficient gas exchange for cell survival. 4) Consider the difference depending on

whether it is suspended cells or adherent cells.

Although cell growth was slightly inhibited in the full-filled media condition compared to the original condition (half-filled media), 1 G and taSMG were performed in the same full-filled media condition and compared. In addition, although the partial pressure of O_2 and CO_2 was not measured to determine whether the gas was exchanged properly, when the pH of the media was measured, it was inferred that the gas was exchanged well even in a full-filled condition.

The findings of this study suggest that taSMG-induced autophagy following the induction of oxidative stress in human HL cells has an anticancer effect. For the scavenger of ROS generation, I confirmed that phenomena of oxidative stress and autophagy were prevented under taSMG. It was thought that taSMG induce ROS production by regulating NADPH oxidase family genes. Interestingly, it was confirmed that these genes are reduced when scavenging the generated ROS by NAC treatment. There are many genes involved in ROS generation, but I have only identified the NADPH oxidase family genes, so it is no yet clear whether taSMG regulates the NADPH oxidase family genes or ROS production. An experiment comparing these genes with knock-down will be necessary as a further study.

taSMG has been shown to affect cancer cells, but not to normal HDF cells. But, the use of HDF cells as normal cells compared to HL cells is inappropriate. So, I confirmed the effect of taSMG on normal lymphocyte pro-B cell and NK cell lines. Unlike the expectation that there will be no change like HDF cells, NK cell growth is inhibited in taSMG. In fact, many studies have

shown that the function of immune cells is inhibited in microgravity[87-93]. Therefore, the results of inhibition of NK cell growth in taSMG are justifiable, and I am working on a follow-up study related to NK cell activity [94]. Ba/F3 cells, a murine pro-B cell line, increased cell growth in taSMG. Whether these results show a difference between murine and human or other effects on B-cells requires further experimentation.

I hypothesized that *in vitro* culture, a change in gravity other than 1 G would be taken as a stress to the cell, so the same experiment was performed on hypergravity (>1 G). There was no change in the growth of HL cells in hypergravity, as opposed to hypothesis that hypergravity would be more extreme stress compared to microgravity. As only cell number was measured, it does not affect growth, but other biological changes may be necessary, and further studies are needed.

This study ought to provide important insight concerning the effect of taSMG on cancer cells, as well as understanding of human HL cell mechanisms. These findings could lead the way to promote new treatment methods for cancer patients.

CONCLUSION

A 3D clinostat, suitable for operation in a conventional incubator, was designed and manufactured. Additionally, optimized angular velocities for symmetric acceleration distribution were determined. The simulation results tested that the 3D clinostat could provide proper taSMG without repeated trajectory of acceleration vector.

The cell culture condition in 3D clinostat system was confirmed, and it is different from the original cell culture methods, but this was excluded by the same control and experimental conditions and could be explained as an effect by taSMG.

In taSMG, inhibition of cell number was confirmed in human breast cancer cells as well was human HL cells, and there was no change in normal HDF cells. The purpose of this study was to confirm the effect of taSMG on human HL cells, which are suspension cells that can further exclude shear flow stress.

In taSMG, human HL cells have increased ROS production, decreased mitochondrial mass, decreased expression of ATPase and ATP synthase, and thereby decreased intracellular ATP level. These cascade demonstrated that taSMG induces autophagy, which occurs through the AMPK/Akt/mTOR and MAPK pathway. This phenomenon was defended by the ROS scavenger, NAC.

In normal HDF cells, taSMG did not change ROS generation and mitochondrial mass. Therefore, it is considered that

additional evidence is needed to explain that cancer cells are more sensitive to taSMG or cancer cell–specifir responses than normal cells.

Since the observation of changes in cancer cells through gravity control was the first goal, additional experiments were performed to measure the number of cancer cells in hypergravity, but no change was confirmed. Therefore, it is considered that the method of simulating microgravity is more suitable for cancer therapy through gravity control. As the age of space travel has arrived, in this research have potential value in the development of new therapies for treating lymphoma.

FUTURE WORK

Based on the current research, the following tasks are suggested on a future work:

1. Identify specific markers that have been exposed to taSMG
2. Confirmation of metabolism change between normal cell and cancer cell in taSMG through analysis such as RNA sequencing, proteomics and metabolite profiling)
3. Investigation of the effect of taSMG on various immune cells
4. Species-specific changes in taSMG: differences between human and mouse cells
5. Cellular signaling pathway verification through genetic engineering
6. Investigation of cell changes in partial gravity such as the moon and mars
7. In vivo test

ACKNOWLEDGMENT

This work was supported by the National Research Foundation of Kore (NRF) funded by the Korean government (NRF-2018M1A3A3A02065779)

REFERENCES

1. Ran, F., et al., *Simulated microgravity potentiates generation of reactive oxygen species in cells.* Biophysics Reports, 2016. **2**(5): p. 100-105.
2. Takeda, M., et al., *Effects of simulated microgravity on proliferation and chemosensitivity in malignant glioma cells.* Neurosci Lett, 2009. **463**(1): p. 54-9.
3. Fitts, R.H., et al., *Prolonged space flight-induced alterations in the structure and function of human skeletal muscle fibres.* J Physiol, 2010. **588**(Pt 18): p. 3567-92.
4. Trappe, S.W., et al., *Comparison of a space shuttle flight (STS-78) and bed rest on human muscle function.* J Appl Physiol (1985), 2001. **91**(1): p. 57-64.
5. Williams, D., et al., *Acclimation during space flight: effects on human physiology.* Cmaj, 2009. **180**(13): p. 1317-23.
6. Foster, J.S., et al., *Impact of simulated microgravity on the normal developmental time line of an animal-bacteria symbiosis.* Sci Rep, 2013. **3**: p. 1340.
7. Wei, L., et al., *Effect of change in spindle structure on proliferation inhibition of osteosarcoma cells and osteoblast under simulated microgravity during incubation in rotating bioreactor.* PLoS One, 2013. **8**(10): p. e76710.
8. Grimm, D., et al., *The impact of microgravity on bone in humans.* Bone, 2016. **87**: p. 44-56.
9. National Aeronautics and Space Administration, C.A.E., Julie A. Robinson, Judy Tate-Brown, Tracy Thumm, Jessica Crespo-Richey, David Baumann, Jennifer Rhatigan *International Space Station Science Research Accomplishments During the Assembly*

Years: An Analysis of Results from 2000-2008. CreateSpace Independent Publishing Platform 2012.

10. Parra, M., et al., *Microgravity validation of a novel system for RNA isolation and multiplex quantitative real time PCR analysis of gene expression on the International Space Station.* PLoS One, 2017. **12**(9): p. e0183480.
11. Brinckmann, E., *New facilities and instruments for developmental biology research in space.* Adv Space Biol Med, 2003. **9**: p. 253-80.
12. Brinckmann, E., *BIOLAB, EPU and EMCS for cell culture experiments on the ISS.* J Gravit Physiol, 2004. **11**(1): p. 67-74.
13. Becker, J.L. and G.R. Souza, *Using space-based investigations to inform cancer research on Earth.* Nat Rev Cancer, 2013. **13**(5): p. 315-27.
14. Villa, A., et al., *Cell behavior in simulated microgravity: a comparison of results obtained with RWV and RPM.* Gravit Space Biol Bull, 2005. **18**(2): p. 89-90.
15. Hatton, J.P., et al., *The kinetics of translocation and cellular quantity of protein kinase C in human leukocytes are modified during spaceflight.* Faseb j, 1999. **13 Suppl**: p. S23-33.
16. Cogoli-Greuter, M., *The Lymphocyte Story - an Overview of Selected Highlights on the in Vitro Activation of Human Lymphocytes in Space.* Microgravity Science and Technology, 2014. **25**: p. 343-352.
17. Schwarzenberg, M., et al., *Signal transduction in T lymphocytes--a comparison of the data from space, the free fall machine and the random positioning machine.* Adv Space Res, 1999. **24**(6): p. 793-800.
18. Walther, I., et al., *Simulated microgravity inhibits the genetic expression of interleukin-2 and its receptor in mitogen-activated*

T lymphocytes. FEBS Lett, 1998. **436**(1): p. 115-8.

19. Maier, J.A., et al., *The impact of microgravity and hypergravity on endothelial cells.* Biomed Res Int, 2015. **2015**: p. 434803.
20. Lin, S.C., et al., *Simulated Microgravity Disrupts Cytoskeleton Organization and Increases Apoptosis of Rat Neural Crest Stem Cells Via Upregulating CXCR4 Expression and RhoA-ROCK1-p38 MAPK-p53 Signaling.* Stem Cells Dev, 2016. **25**(15): p. 1172-93.
21. Blaber, E.A., et al., *Microgravity Reduces the Differentiation and Regenerative Potential of Embryonic Stem Cells.* Stem Cells Dev, 2015. **24**(22): p. 2605-21.
22. Feger, B.J., et al., *Microgravity induces proteomics changes involved in endoplasmic reticulum stress and mitochondrial protection.* Sci Rep, 2016. **6**: p. 34091.
23. Chung, J.H., et al., *Simulated Microgravity Effects on Nonsmall Cell Lung Cancer Cell Proliferation and Migration.* Aerosp Med Hum Perform, 2017. **88**(2): p. 82-89.
24. Arun, R.P., et al., *PTEN/FOXO3/AKT pathway regulates cell death and mediates morphogenetic differentiation of Colorectal Cancer Cells under Simulated Microgravity.* Sci Rep, 2017. **7**(1): p. 5952.
25. Zhao, T., et al., *Simulated Microgravity Promotes Cell Apoptosis Through Suppressing Uev1A/TICAM/TRAF/NF-κB-Regulated Anti-Apoptosis and p53/PCNA- and ATM/ATR-Chk1/2-Controlled DNA-Damage Response Pathways.* J Cell Biochem, 2016. **117**(9): p. 2138-48.
26. Kopp, S., et al., *Identifications of novel mechanisms in breast cancer cells involving duct-like multicellular spheroid formation after exposure to the Random Positioning Machine.* Sci Rep, 2016. **6**: p. 26887.

27. Riwaldt, S., et al., *Pathways Regulating Spheroid Formation of Human Follicular Thyroid Cancer Cells under Simulated Microgravity Conditions: A Genetic Approach.* Int J Mol Sci, 2016. **17**(4): p. 528.

28. Adrian, A., et al., *The oxidative burst reaction in mammalian cells depends on gravity.* Cell Commun Signal, 2013. **11**: p. 98.

29. Verhaar, A.P., et al., *Dichotomal effect of space flight-associated microgravity on stress-activated protein kinases in innate immunity.* Sci Rep, 2014. **4**: p. 5468.

30. Morabito, C., et al., *Transient increases in intracellular calcium and reactive oxygen species levels in TCam-2 cells exposed to microgravity.* Sci Rep, 2017. **7**(1): p. 15648.

31. Poillet-Perez, L., et al., *Interplay between ROS and autophagy in cancer cells, from tumor initiation to cancer therapy.* Redox Biol, 2015. **4**: p. 184-92.

32. Filomeni, G., D. De Zio, and F. Cecconi, *Oxidative stress and autophagy: the clash between damage and metabolic needs.* Cell Death Differ, 2015. **22**(3): p. 377-88.

33. Sambandam, Y., et al., *Microgravity control of autophagy modulates osteoclastogenesis.* Bone, 2014. **61**: p. 125-31.

34. Lee, J., S. Giordano, and J. Zhang, *Autophagy, mitochondria and oxidative stress: cross-talk and redox signalling.* Biochem J, 2012. **441**(2): p. 523-40.

35. Pal, R., et al., *Src-dependent impairment of autophagy by oxidative stress in a mouse model of Duchenne muscular dystrophy.* Nat Commun, 2014. **5**: p. 4425.

36. Wang, Q., et al., *2-Deoxy-D-glucose treatment of endothelial cells induces autophagy by reactive oxygen species-mediated activation of the AMP-activated protein kinase.* PLoS One, 2011. **6**(2): p. e17234.

37. Sureshbabu, A., S.W. Ryter, and M.E. Choi, *Oxidative stress and autophagy: crucial modulators of kidney injury.* Redox Biol, 2015. **4**: p. 208-14.

38. Xie, Z. and D.J. Klionsky, *Autophagosome formation: core machinery and adaptations.* Nat Cell Biol, 2007. **9**(10): p. 1102-9.

39. Yu, Y., et al., *Akt/AMPK/mTOR pathway was involved in the autophagy induced by vitamin E succinate in human gastric cancer SGC-7901 cells.* Mol Cell Biochem, 2017. **424**(1-2): p. 173-183.

40. He, C. and D.J. Klionsky, *Regulation mechanisms and signaling pathways of autophagy.* Annu Rev Genet, 2009. **43**: p. 67-93.

41. Kim, J., et al., *AMPK and mTOR regulate autophagy through direct phosphorylation of Ulk1.* Nat Cell Biol, 2011. **13**(2): p. 132-41.

42. Shaw, R.J., *LKB1 and AMP-activated protein kinase control of mTOR signalling and growth.* Acta Physiol (Oxf), 2009. **196**(1): p. 65-80.

43. Grandér, D. and T. Panaretakis, *Autophagy: cancer therapy's friend or foe?* Future Med Chem, 2010. **2**(2): p. 285-97.

44. Laane, E., et al., *Cell death induced by dexamethasone in lymphoid leukemia is mediated through initiation of autophagy.* Cell Death Differ, 2009. **16**(7): p. 1018-29.

45. Buentke, E., et al., *Glucocorticoid-induced cell death is mediated through reduced glucose metabolism in lymphoid leukemia cells.* Blood Cancer J, 2011. **1**(7): p. e31.

46. Thorburn, A., D.H. Thamm, and D.L. Gustafson, *Autophagy and cancer therapy.* Mol Pharmacol, 2014. **85**(6): p. 830-8.

47. Yang, Z.J., et al., *The role of autophagy in cancer: therapeutic implications.* Mol Cancer Ther, 2011. **10**(9): p. 1533-41.

48. Sui, X., et al., *Autophagy and chemotherapy resistance: a promising therapeutic target for cancer treatment.* Cell Death Dis, 2013. **4**(10): p. e838.

49. *Surveillance, Epidemiology, and End Results Program. Cancer Strat Facts: Hodgkin Lymphoma.* NIH. National Cancer Institute, 2018.

50. Eichenauer, D.A., et al., *Therapy-related acute myeloid leukemia and myelodysplastic syndromes in patients with Hodgkin lymphoma: a report from the German Hodgkin Study Group.* Blood, 2014. **123**(11): p. 1658-64.

51. Rutenberg, M.S., S. Flampouri, and B.S. Hoppe, *Proton therapy for Hodgkin lymphoma.* Curr Hematol Malig Rep, 2014. **9**(3): p. 203-11.

52. Franklin, J., et al., *Optimisation of chemotherapy and radiotherapy for untreated Hodgkin lymphoma patients with respect to second malignant neoplasms, overall and progression-free survival: individual participant data analysis.* Cochrane Database Syst Rev, 2017. **9**(9): p. Cd008814.

53. Canellos, G.P., et al., *Chemotherapy of advanced Hodgkin's disease with MOPP, ABVD, or MOPP alternating with ABVD.* N Engl J Med, 1992. **327**(21): p. 1478-84.

54. Duggan, D.B., et al., *Randomized comparison of ABVD and MOPP/ABV hybrid for the treatment of advanced Hodgkin's disease: report of an intergroup trial.* J Clin Oncol, 2003. **21**(4): p. 607-14.

55. Chisesi, T., et al., *Long-term follow-up analysis of HD9601 trial comparing ABVD versus Stanford V versus MOPP/EBV/CAD in patients with newly diagnosed advanced-stage Hodgkin's lymphoma: a study from the Intergruppo Italiano Linfomi.* J Clin Oncol, 2011. **29**(32): p. 4227-33.

56. Engert, A., et al., *Reduced-intensity chemotherapy and PET-guided radiotherapy in patients with advanced stage Hodgkin's lymphoma (HD15 trial): a randomised, open-label, phase 3 non-inferiority trial.* Lancet, 2012. **379**(9828): p. 1791-9.

57. Song, E.J., et al., *Consolidation Radiation Therapy for Patients With Advanced Hodgkin Lymphoma in Complete Metabolic Response According to PET-CT or Gallium Imaging.* Clin Lymphoma Myeloma Leuk, 2018. **18**(2): p. 145-151.

58. Kim, Y.J., et al., *Time-averaged simulated microgravity (taSMG) inhibits proliferation of lymphoma cells, L-540 and HDLM-2, using a 3D clinostat.* Biomed Eng Online, 2017. **16**(1): p. 48.

59. Jeong, A.J., et al., *Microgravity induces autophagy via mitochondrial dysfunction in human Hodgkin's lymphoma cells.* Sci Rep, 2018. **8**(1): p. 14646.

60. Kim, B.H., et al., *A small-molecule compound identified through a cell-based screening inhibits JAK/STAT pathway signaling in human cancer cells.* Mol Cancer Ther, 2008. **7**(9): p. 2672-80.

61. Shi, Z.X., et al., *Modeled microgravity suppressed invasion and migration of human glioblastoma U87 cells through downregulating store-operated calcium entry.* Biochem Biophys Res Commun, 2015. **457**(3): p. 378-84.

62. Masiello, M.G., et al., *Phenotypic switch induced by simulated microgravity on MDA-MB-231 breast cancer cells.* Biomed Res Int, 2014. **2014**: p. 652434.

63. Li, J., et al., *Modeled microgravity causes changes in the cytoskeleton and focal adhesions, and decreases in migration in malignant human MCF-7 cells.* Protoplasma, 2009. **238**(1-4): p. 23-33.

64. Antico Arciuch, V.G., et al., *Mitochondrial regulation of cell cycle and proliferation.* Antioxid Redox Signal, 2012. **16**(10): p. 1150-

80.

65. Yan, X.J., et al., *Mitochondria play an important role in the cell proliferation suppressing activity of berberine.* Sci Rep, 2017. **7**: p. 41712.

66. Holmuhamedov, E., et al., *Suppression of human tumor cell proliferation through mitochondrial targeting.* Faseb j, 2002. **16**(9): p. 1010-6.

67. Meitzler, J.L., et al., *NADPH oxidases: a perspective on reactive oxygen species production in tumor biology.* Antioxid Redox Signal, 2014. **20**(17): p. 2873-89.

68. Chen, S., X.F. Meng, and C. Zhang, *Role of NADPH oxidase-mediated reactive oxygen species in podocyte injury.* Biomed Res Int, 2013. **2013**: p. 839761.

69. Bedard, K. and K.H. Krause, *The NOX family of ROS-generating NADPH oxidases: physiology and pathophysiology.* Physiol Rev, 2007. **87**(1): p. 245-313.

70. Apostolova, N. and V.M. Victor, *Molecular strategies for targeting antioxidants to mitochondria: therapeutic implications.* Antioxid Redox Signal, 2015. **22**(8): p. 686-729.

71. Aparicio, I.M., et al., *Autophagy-related proteins are functionally active in human spermatozoa and may be involved in the regulation of cell survival and motility.* Sci Rep, 2016. **6**: p. 33647.

72. Kadowaki, M. and M.R. Karim, *Cytosolic LC3 ratio as a quantitative index of macroautophagy.* Methods Enzymol, 2009. **452**: p. 199-213.

73. Wang, Y., et al., *Loss of macroautophagy promotes or prevents fibroblast apoptosis depending on the death stimulus.* J Biol Chem, 2008. **283**(8): p. 4766-77.

74. Shackelford, D.B. and R.J. Shaw, *The LKB1-AMPK pathway: metabolism and growth control in tumour suppression.* Nat Rev

Cancer, 2009. **9**(8): p. 563-75.

75. Son, Y., et al., *Mitogen-Activated Protein Kinases and Reactive Oxygen Species: How Can ROS Activate MAPK Pathways?* J Signal Transduct, 2011. **2011**: p. 792639.

76. Torres, M. and H.J. Forman, *Redox signaling and the MAP kinase pathways.* Biofactors, 2003. **17**(1-4): p. 287-96.

77. Valko, M., et al., *Free radicals and antioxidants in normal physiological functions and human disease.* Int J Biochem Cell Biol, 2007. **39**(1): p. 44-84.

78. Zhou, Y.Y., et al., *MAPK/JNK signalling: a potential autophagy regulation pathway.* Biosci Rep, 2015. **35**(3).

79. Wuest, S.L., et al., *A Novel Microgravity Simulator Applicable for Three-Dimensional Cell Culturing.* Microgravity Science and Technology, 2014. **26**(2): p. 77-88.

80. Lowry, L., P. Hoskin, and D. Linch, *Developments in the management of Hodgkin's lymphoma.* Lancet, 2010. **375**(9717): p. 786-8.

81. Stein, H., et al., *Down-regulation of BOB.1/OBF.1 and Oct2 in classical Hodgkin disease but not in lymphocyte predominant Hodgkin disease correlates with immunoglobulin transcription.* Blood, 2001. **97**(2): p. 496-501.

82. Berglund, M., et al., *Molecular cytogenetic characterization of four commonly used cell lines derived from Hodgkin lymphoma.* Cancer Genet Cytogenet, 2003. **141**(1): p. 43-8.

83. Tian, Y., et al., *The Impact of Oxidative Stress on the Bone System in Response to the Space Special Environment.* Int J Mol Sci, 2017. **18**(10).

84. Stein, T.P. and M.J. Leskiw, *Oxidant damage during and after spaceflight.* Am J Physiol Endocrinol Metab, 2000. **278**(3): p. E375-82.

85. Mao, X.W., et al., *Role of NADPH Oxidase as a Mediator of Oxidative Damage in Low-Dose Irradiated and Hindlimb-Unloaded Mice.* Radiat Res, 2017. **188**(4): p. 392-399.
86. Yoo, Y.M., T.Y. Han, and H.S. Kim, *Melatonin Suppresses Autophagy Induced by Clinostat in Preosteoblast MC3T3-E1 Cells.* Int J Mol Sci, 2016. **17**(4): p. 526.
87. Cervantes, J.L. and B.Y. Hong, *Dysbiosis and Immune Dysregulation in Outer Space.* Int Rev Immunol, 2016. **35**(1): p. 67-82.
88. Borchers, A.T., C.L. Keen, and M.E. Gershwin, *Microgravity and immune responsiveness: implications for space travel.* Nutrition, 2002. **18**(10): p. 889-98.
89. Chen, Y., et al., *Effect of Long-Term Simulated Microgravity on Immune System and Lung Tissues in Rhesus Macaque.* Inflammation, 2017. **40**(2): p. 589-600.
90. Zayzafoon, M., V.E. Meyers, and J.M. McDonald, *Microgravity: the immune response and bone.* Immunol Rev, 2005. **208**: p. 267-80.
91. Mukhopadhyay, S., et al., *A systems biology pipeline identifies new immune and disease related molecular signatures and networks in human cells during microgravity exposure.* Sci Rep, 2016. **6**: p. 25975.
92. Van Walleghem, M., et al., *Gravity-Related Immunological Changes in Human Whole Blood Cultured Under Simulated Microgravity Using an In Vitro Cytokine Release Assay.* J Interferon Cytokine Res, 2017. **37**(12): p. 531-540.
93. Tascher, G., et al., *Analysis of femurs from mice embarked on board BION-M1 biosatellite reveals a decrease in immune cell development, including B cells, after 1 wk of recovery on Earth.* Faseb j, 2019. **33**(3): p. 3772-3783.

94. Kim, Y.J., et al., *Manufacturing and Control of a Robotic Device for Time-averaged Simulated Micro and Partial Gravity of a Cell Culture Environment.* International Journal of Control, Automation and Systems, 2020. **18**(1): p. 53-64.

국문 초록

중력은 항상성을 유지하는 기능으로 인체에 물리적 스트레스를 가할 수 있다. 미세중력을 경험한 우주 비행사는 다양한 생물학적 기능들이 변화된다는 보고가 있으며, 이러한 미세중력의 영향에 대해 많은 연구들이 진행 중이다. 지구에서 미세중력을 모사하는 환경을 제공하는 시스템인 클리노스탯을 이용하여 많은 후속연구가 수행되고 있다. 그러나 아직까지 미세중력 모사 환경의 다양한 세포학적 변화 메커니즘은 여전히 명확하지 않다. 그래서 이 연구에서는 시간-평균 미세중력 모사 환경(taSMG)을 제공하는 3D clinostat을 이용하여 인간 호지킨 림프종세포의 변화를 관찰하였다.

호지킨 림프종 세포의 증식이 3 일동안 taSMG 에서 배양 될 때 억제되는 반면, 정상 인간 진피 섬유아세포의 증식에는 영향을 미치지 않음을 관찰하였다. 그런 다음 taSMG 가 항암 효과를 가지는지 확인하고자, 2 일동안 인간 호지킨 림프종 세포를 taSMG 에 노출 시켰다. 활성산소종(ROS) 생성 및 NADPH 산화효소 패밀리 유전자 발현이 증가되는 반면, 미토콘드리아 질량, ATP 분해효소, ATP 합성효소 및 세포 내 ATP 수준이 감소되었다. 또한, taSMG 에 노출된 인간 호지킨 림프종 세포는 AMPK/AKT/mTOR 및 MAPK 신호전달 경로를 조절하여 자가 포식을 하게되고; 이러한 자가 포식은 ROS 스캐빈저인 *N*-아세틸 시스테인(NAC)에 의해 억제되었다.

우주를 여행하거나 지구에서 미세중력을 모사하는 방법이 좀 더 발달하면, 이러한 연구 결과는 기존의 화학 요법 및 방사선 요법과 다른 호지킨 림프종에 대한 새로운 치료법으로 가치가 있음을 시사한다.

주요어 : 중력, 3 차원 클리노스탯, 시간-평균 미세중력 모사 환경, 호지킨 림프종, 미토콘드리아 기능 장애, 활성산소 생성, 자가포식

학 번 : 2015-30609